Sodium Ion Batteries | Special Issue 150 Years of BASF

DOI: 10.1002/anie.201410376

The Emerging Chemistry of Sodium Ion Batteries for Electrochemical Energy Storage

*Dipan Kundu, Elahe Talaie, Victor Duffort, and Linda F. Nazar**

Keywords:
anodes · cathodes · energy storage · grid storage · sodium ion batteries

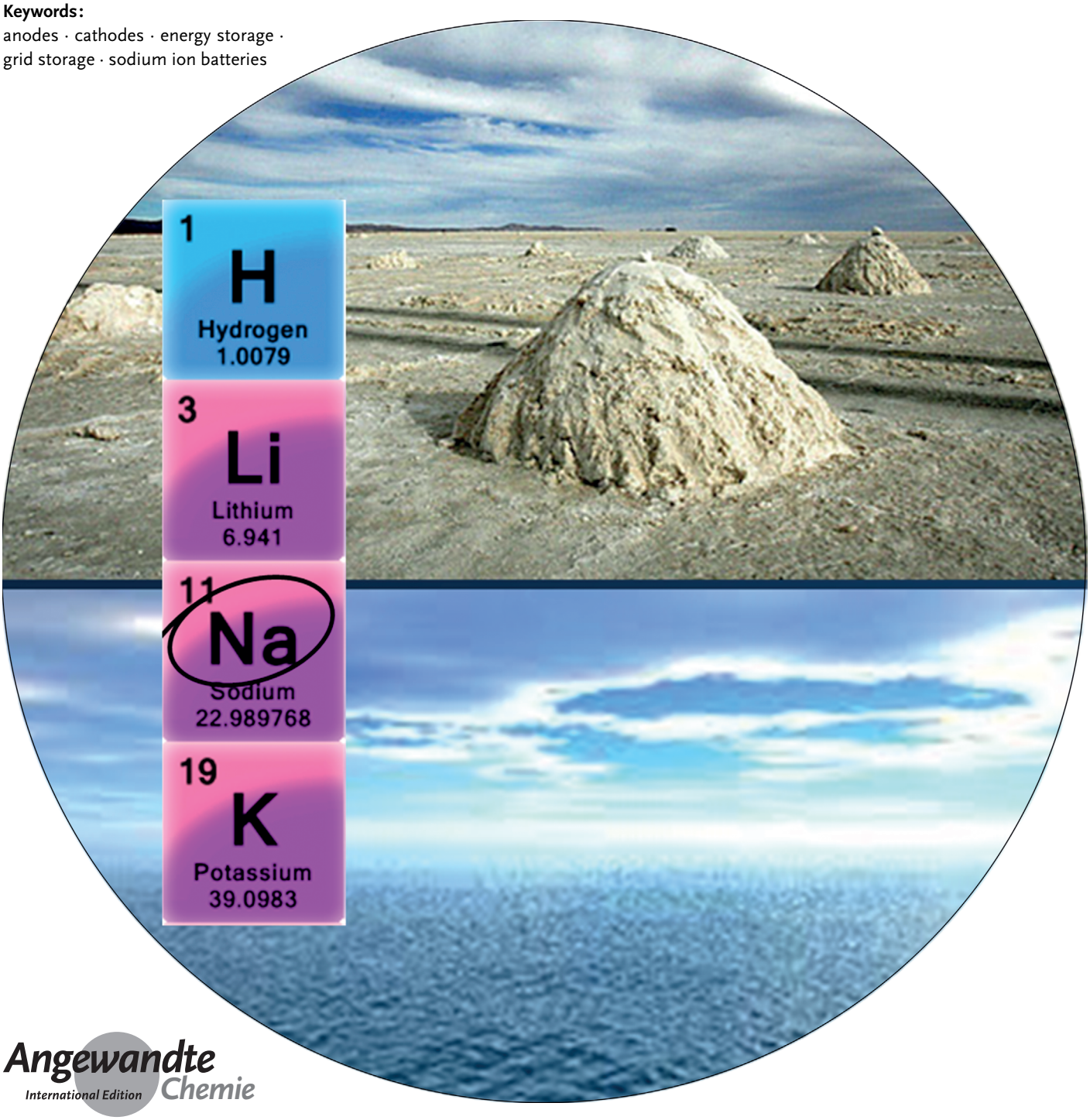

Angewandte International Edition Chemie

Energy storage technology has received significant attention for portable electronic devices, electric vehicle propulsion, bulk electricity storage at power stations, and load leveling of renewable sources, such as solar energy and wind power. Lithium ion batteries have dominated most of the first two applications. For the last two cases, however, moving beyond lithium batteries to the element that lies below—sodium—is a sensible step that offers sustainability and cost-effectiveness. This requires an evaluation of the science underpinning these devices, including the discovery of new materials, their electrochemistry, and an increased understanding of ion mobility based on computational methods. The Review considers some of the current scientific issues underpinning sodium ion batteries.

From the Contents

1. Introduction

Energy storage has become a growing global concern over the past decade as a result of increased energy demand, combined with increases in the price of refined fossil fuels and the environmental consequences of their use. This has increased the call for environmentally responsible alternative sources for both energy generation and storage. Of the several technologies that are suitable for large-scale energy storage, pumped hydroelectric systems currently dominate, with compressed air being the second most utilized system. However, electrochemical energy storage (EES) technologies based on batteries are beginning to show considerable promise as a result of many breakthroughs in the last few years. Their appealing features include high round-trip efficiency, flexible power, and energy characteristics to meet different grid functions, long cycle life, and low maintenance. Batteries, in particular, represent a viable energy storage technology for the integration of renewable resources that provide intermittent energy into the grid. These include solar energy from photovoltaics and wind energy (Figure 1). The compact size of battery systems makes them well-suited for use at distributed locations (off-grid or minigrid), where they can provide energy storage for local solar output that can be used to charge an electric/hybrid electric vehicle (EV/HEV), supply energy for residential use, or enable electrification of entire rural communities. On-grid, batteries are utilized to store and manage peak load energy from large photovoltaic power plants and load-level output fluctuations at wind farms. The storage can be used to feed power to the grid when consumption exceeds regular production, and/or utilized for off-peak utilization such as for EV charging.

Energy storage for the electrical grid has primarily been focussed on lithium ion (Li ion), redox-flow, and high-temperature batteries up to now. Of these, Li ion EES is certainly a contender. Nonetheless, the demand for Li ion batteries as a major power source in portable electronic devices and vehicles is rapidly increasing. Li-ion cells are now powering hybrid-electric and plug-in electric vehicles and are forecast to continue to be the energy storage system for future generations.[1] In the face of greatly increased demands on available global lithium resources because of the eventual rise in these markets, concerns over potentially rising costs and availability have arisen. Most easily accessible global lithium reserves are in remote or in politically sensitive areas.[2–4] Increasing utilization of lithium in energy storage applications with a higher "price point" will ultimately push up the price of lithium compounds even with extensive battery recycling programs thereby making large-scale storage based on this element less affordable. Limitations in the availability of the transition metals for cathode materials are also of concern,

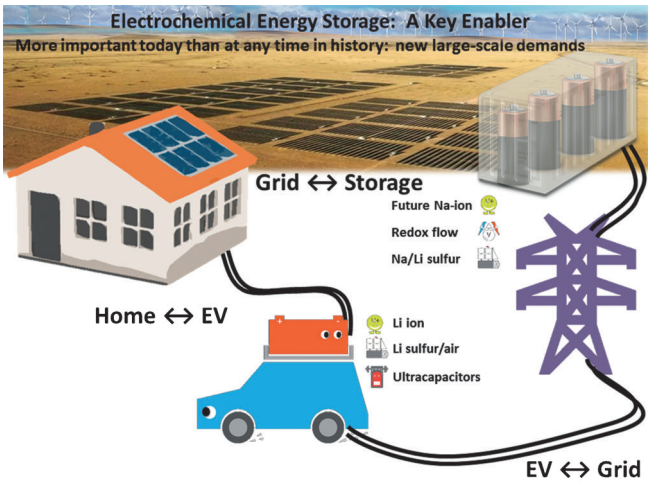

Figure 1. A unified model for the grid and microgrid, showing the interplay between renewable energy generation that supplies the grid, energy storage solutions for the grid, and energy supply for hybrid/electric vehicle transport.

[*] Dr. D. Kundu,[+] E. Talaie,[+] Dr. V. Duffort,[+] Prof. L. F. Nazar
Department of Chemistry & Waterloo Institute for Nanotechnology
University of Waterloo
200 University Avenue West, Waterloo, Ontario, N2L 3G1 (Canada)
E-mail: lfnazar@uwaterloo.ca

[+] These authors contributed equally to this work.

driving development towards more sustainable elements such as Fe and Mn.

Given the high abundance and low cost of sodium as well as its very suitable redox potential ($E^{o}_{(Na+/Na)} = -2.71$ V versus the standard hydrogen electrode) which is only 0.3 V above that of lithium, meaning there is only a small energy penalty to pay—rechargeable electrochemical cells based on sodium hold much more promise for EES applications. The electrochemistry of sodium materials has a long history. Fifty years ago, the discovery of the high-temperature solid-state sodium ionic conductor $NaAl_{11}O_{17}$ (β"-alumina) provided a leap forward in the fields of solid-state ionics and sodium electrochemistry,[5] along with NASICON (natrium super ion conductor: $Na_xM_2(XO_4)_3$; $X = P^{5+}$, Si^{4+}, S^{6+}, Mo^{6+}, As^{5+}) a decade later.[6] As a solid-state electrolyte, β"-alumina was critical to the development of two sodium ion batteries: the sodium/sulfur (Na-S) and ZEBRA cells (zero-emission battery research activities) that are based on $Na/NiCl_2$. These cells, particularly the former, are now commercial technologies used today for grid storage. They operate near 300 °C, where sodium and the positive electrodes are molten, and the ion conductivity of the sodium β"-alumina membrane is enhanced. Safety concerns with Na/S technology, and costly heating requirements and temperature management difficulties in ZEBRA cells are inspiring much effort to lower their operating temperatures. NASICON has been exploited as a solid-state electrolyte membrane for Na batteries that operate between 110 and 130 °C and which also encompass a molten sodium electrode.[7] Fundamental research in solid-state Na ion conductors has lowered the operating temperature even further. Room-temperature operation of an all-solid-state rechargeable sodium battery based on a sulfide glass-ceramic electrolyte has recently been demonstrated.[8] This brings the exciting possibility of a room-temperature Na/S cell closer to reality, although further developments are necessary.

On the other hand, sodium ion batteries (NIBs) based on intercalation materials that employ non-aqueous electrolytes—akin to lithium ion batteries—were first explored in the mid-1980s. They have undergone a renaissance in the last few years, with a remarkable number of new materials and approaches having been reported. They offer a higher energy density than aqueous batteries and lower cost than Li ion batteries, with some now approaching the energy density of the latter. Here, we discuss recent research highlights of sodium ion based electrochemistry, with a focus on recent studies on intercalation compounds for positive electrode materials (layered transition-metal oxides and polyanionic compounds); computational studies that probe Na^+ ion mobility in solid-state lattices; developments in open-framework materials; and negative electrode materials (hard carbons, alloys, and metal oxides). A brief overview on the research of non-aqueous and ionic liquid-based electrolytes is also presented. We note that a few excellent review articles have appeared in 2012 and 2013,[9–12] so our emphasis is on the most recent significant issues and opportunities provided by the field. Although aqueous Na ion batteries also have several apparent advantages for large-scale storage, a comprehensive review on this topic has just been published,[13] and we refer the reader there.

2. Overview of the Sodium Ion Cell

The development of sodium ion cells paralleled that of Li ion batteries through the 1980s.[14–21] The higher energy density of the lithium counterparts—owing to their higher

Dipan Kundu received his PhD in 2012 from the ETH Zürich in the group of Prof. Reinhard Nesper. Currently, he is a postdoctoral researcher in the group of Prof. Linda F. Nazar at the University of Waterloo. His research interests are in functional material development for electrochemical energy storage applications, in particular of Na ion and Li-O_2 batteries.

Victor Duffort received his PhD in 2012 from the Université de Caen Basse-Normandie, France, on the oxygen stoichiometry and structural characterization of magnetic iron oxides. He joined the group of Prof. Linda F. Nazar in 2013, and has been focusing on the development of alternative technologies to Li ion batteries. His currents research interests reside in the discovery of new cathode materials for sodium and magnesium batteries.

Elahe Talaie is carrying out PhD research (electrical engineering; Nanotechnology program) at the University of Waterloo under the supervision of Prof. Linda F. Nazar. Since 2010 she has been actively involved in the development of cathode materials for Li ion and Na ion batteries. She currently works on the synthesis and characterization of layered oxides as cathode materials for Na ion batteries.

Linda Nazar was born in Vancouver, Canada, and received her PhD from the University of Toronto. After a postdoctoral fellowship at Exxon Corporate Research in Annandale, New Jersey, she moved to the University of Waterloo, where she is a Professor of Chemistry and Electrical Engineering, and a fellow of the Royal Society of Canada. She holds a Senior Canada Research Chair in Solid-State Energy Materials. Her research focuses on nanostructured intercalation electrodes for sodium ion batteries, solid-state electrolytes/batteries, and Li-S and Li-O_2 batteries.

potential and lower mass—resulted in their domination of both research and commercial fields, and led to the exponential growth in the portable electronics market in the 1990s. However, for stationary applications, where gravimetric energy density is not so much of a concern (such as grid or minigrid storage), Na ion batteries are an equally viable technology. Recent reports have even shown that these cells can compete with Li ion batteries in terms of energy density (see Section 3.1). Nonetheless, several barriers need to be overcome before such cells can become a practical, commercial reality. Depending on the cell chemistry, these barriers include insufficient cycle life and the need for the discovery of new materials for both the positive (and especially) negative electrodes to increase the performance. Research in sodium ion batteries has increased dramatically in the last few years and is now in full-swing to address these hurdles and thereby enable this emerging energy storage technology to become available in the coming years.

The principle of cell operation is the same as its Li ion cousin: sodium ions are shuttled between the positive (cathode) and negative (anode) electrodes through a non-aqueous (or aqueous) Na ion electrolyte that is contained between the electrodes (Figure 2) on discharge and charge.[11]

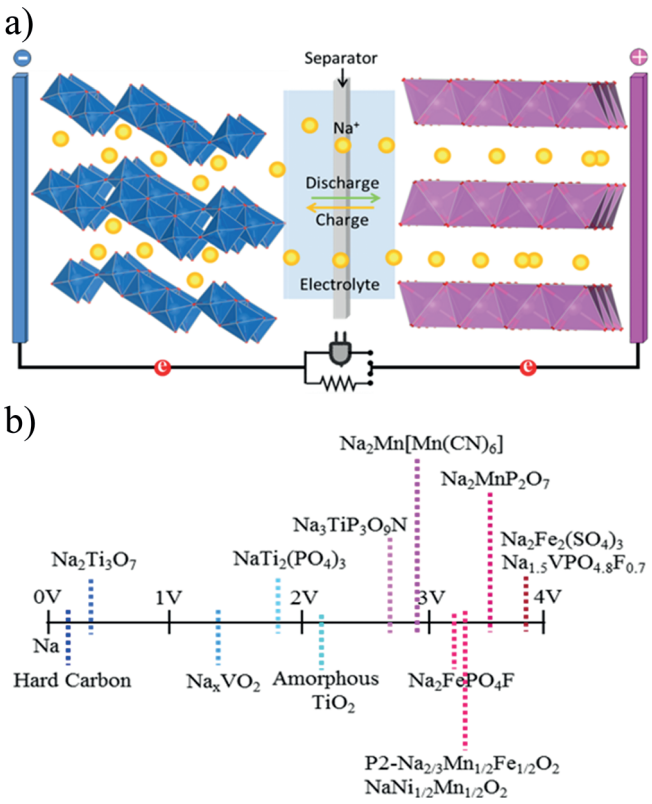

Figure 2. a) Operating principle of a typical non-aqueous or aqueous sodium-ion battery. Sodium ions migrate back and forth in the electrolyte between the negative and positive electrodes upon discharge or charge, and electron flow counterbalances the ion flow within the electrode materials and externally through the outer electrical circuit. The potential difference between the positive and negative electrodes defines the cell voltage. b) Relative working potential of typical electrode materials for non-aqueous and aqueous sodium-ion batteries.

A typical working system is illustrated, where the Na^+ ion electrolyte is a non-aqueous system comprised, for example, of $NaClO_4$ in a polar solvent such as propylene carbonate. During charge, sodium ions are extracted from the high voltage positive electrode, with a working potential around or above 3.0 V versus Na^+/Na (see Figure 2b), and are inserted into the low voltage negative electrode, whose working potential is ideally lower than 1.0 V versus Na^+/Na (see Figure 2b). On charge, the electrons are pumped "uphill", thermodynamically speaking, from the positive to the negative electrode through the external circuit. The converse occurs on discharge: the favorable free energy of the redox couple allows the reaction to proceed "downhill", thus delivering energy to the device that is being powered by the battery.

Full Na ion cells do not employ elemental sodium as the negative electrode: they are comprised of hard carbons or metal oxide intercalation compounds. The negative electrode is one of the most troublesome components because typical graphitic carbons employed in Li ion cells do not intercalate Na^+ ions (Section 5.1). The discovery of suitable anode materials is a major challenge. Furthermore, the Na^+ ions are not reversibly shuttled between the electrodes with 100% Coulombic efficiency because of side reactions between the electrolyte and electrode surface. These can arise by reaction of the electrolyte with the oxidizing transition-metal oxide formed at the cathode, and/or with the highly reducing sodiated hard carbon (or low-potential metal oxide) generated at the anode. For practical cells, these hurdles must be overcome. The next section starts with the outstanding recent developments in positive electrode materials by a variety of approaches, and the challenges that are still to be faced in this "high potential" area.

3. Cathode Materials for High Performance Sodium ion Batteries

3.1. Layered Sodium Transition-Metal Oxides

Major efforts have been devoted to the search for high-performance cathode materials in layered systems of the type AMO_2 (solid solutions of $NaCoO_2$, $NaMnO_2$, $NaFeO_2$, $NaNiO_2$).[22–25] These materials are sought after for their high redox potentials and energy densities. The driving force, at least in part, derives from several advantages associated with low-cobalt-content materials, especially those based on environmentally friendly iron and manganese.

Sodium metal oxides exist as one of several polytypes which differ in the stacking of the close-packed oxygen layers. Following the notation of Delmas,[26] these are designated as O3 (ABCABC stacking), P2 (ABBA stacking), and P3 (ABBCCA stacking). The Na^+ ion adopts different coordination environments (P = prismatic and O = octahedral) depending on the polytype. $NaMO_2$ materials (unlike their lithium analogues) readily form the "ideal" ordered O3-type layered structure as a result of the large difference in the ionic sizes of the Na^+ and the transition-metal cations, which drives the segregation of the A and M into alternating layers. The

vacancy-dominated P2-type $Na_{0.67}MO_2$ oxides are also of considerable interest. Early work demonstrated that P2-type $Na_{0.66}Co_{0.66}Mn_{0.33}O_2$ displays predominantly solid-solution behavior on extraction of the sodium.[27] Recent reports have highlighted manganese and iron oxides, and their combinations with a ternary element; these materials have been shown to be amongst the most viable for positive electrodes, as discussed below.

Layered $NaMnO_2$, one of the first materials investigated, exhibits two structures,[28,29] but α-$NaMnO_2$ is more stable.[30] It crystallizes in the O3 structure. Investigation of its electrochemical properties showed that 0.8 Na can be reversibly de/intercalated with good capacity retention, equivalent to a capacity of 200 mAh g^{-1}.[31] The voltage profiles exhibit pronounced stepwise processes indicative of structural transitions. These are more common in Na ion than in Li ion intercalation oxides because of Na-vacancy ordering interactions which are stronger due to the larger radius of a sodium cation. These involve the gliding of oxygen planes to accommodate Na in both octahedral and trigonal prismatic environments. The latter can only be achieved in an O3 stacking by sliding some of the oxygen layers. Gliding of the oxygen layer also allows optimization of Na coordination at each stoichiometry—which is a stronger driving force than in the lithiated oxides.

P2-$Na_{2/3}Mn_{1/2}Fe_{1/2}O_2$, one of the most promising positive electrode materials for Na ion batteries in terms of both sustainability and electrochemical performance, was studied first by Komaba and co-workers.[32] In addition to the low cost of manganese and iron, P2-$Na_{0.67}Mn_{1/2}Fe_{1/2}O_2$/Na delivers a high specific capacity of about 190 mAh g^{-1} and a specific energy over 520 Wh kg^{-1} (Figure 3). This is comparable to $LiFePO_4$, which exhibits a practical cathode energy density of about 530 Wh kg^{-1}.

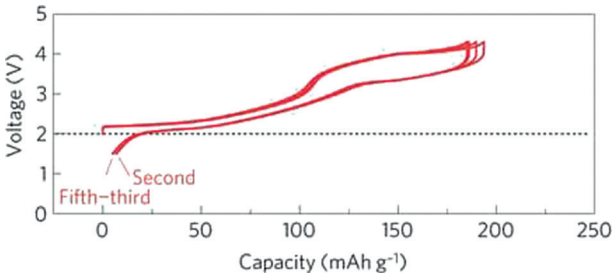

Figure 3. Galvanostatic charge/discharge curve of P2-$Na_{2/3}Mn_{1/2}Fe_{1/2}O_2$ in a Na cell cycled in the voltage range of 1.5–4.3 V at a rate of 12 mA g^{-1}. Reproduced from Ref. [32] with permission. Copyright 2012, Nature Publishing Group.

The cell retains about 70 % of its reversible capacity when the cycling rate is increased from C/20 to 1 C. The superior rate capability of P2-$Na_{2/3}Mn_{1/2}Fe_{1/2}O_2$ compared to that of many other layered transition metal oxides is correlated to its smooth charge/discharge voltage profile, which suggests a facile de/intercalation reaction and the lack of pronounced structural transitions. These dominate in Na_xCoO_2, for example.[33] P2-$Na_{2/3}Mn_{1/2}Fe_{1/2}O_2$ retains over 75 % of its initial capacity after 30 cycles. Capacity fade is attributed to the phase transition from P2 to OP4 upon charge. As evidenced by X-ray absorption spectroscopy and Mössbauer spectroscopy, the Fe^{3+}/Fe^{4+} redox couple is active in the desodiation processes of P2-$Na_{2/3}Mn_{1/2}Fe_{1/2}O_2$ (in contrast to lithium iron oxides where oxygen evolution seems to be the favorable process at high potentials).[34] This auspicious material shows much promise for future development, but the exact charge compensation mechanism is not fully resolved to date. Assuming a Mn^{4+} oxidation state in the charged sample (4.2 V, $x = 0.13$ in $Na_xMn_{0.5}Fe_{0.5}O_2$), more than 70 % of the iron ions are expected to be oxidized on the basis of charge balance ($Na_{0.13}Mn^{+4}{}_{0.5}Fe^{+4}{}_{0.37}Fe^{+3}{}_{0.13}O_2$). However, much less Fe^{4+} was detected by Mössbauer spectroscopy in the sample charged to 4.5 V. Therefore, the extraction of sodium from P2-$Na_xMn_{0.5}Fe_{0.5}O_2$ may be accompanied by one or more charge-compensation mechanisms; most possibly oxygen removal and/or oxidation of manganese ions to higher oxidation states than tetravalent. These unresolved questions inspire further exploration for in-depth understanding of these systems.

In the search for electrode materials with stabilities acceptable for practical Na ion batteries, Meng and co-workers conducted a comprehensive study on the effect of Li substitution on the structural and electrochemical properties of a P2 structured binary system, $Na_x[Li_yNi_zMn_{1-y-z}]O_2$ ($0 < x,y,z < 1$).[35] A smooth voltage profile over the entire range of cycling is exhibited by P2-$Na_{0.8}[Li_{0.12}Ni_{0.22}Mn_{0.66}]O_2$, which indicates sodium de/intercalation through a solid-solution process, in contrast to its structural analogue, $Na_{2/3}[Ni_{1/3}Mn_{2/3}]O_2$. The cell delivers a capacity of 115 mAh g^{-1} between 2.0 and 4.4 V, with excellent retention (91 % after 50 cycles) and rate capability. In situ synchrotron X-ray diffraction registered no phase transition in the structure upon charging up to 4.4 V, although the broadening of peaks on charging implies emerging local stacking faults as a result of in-plane glide. Delay in the occurrence of the P2-O2 phase transition is explained by the presence of more Na^+ ions in the structure (including at the charged state) because of substitution of low-valence Li ions ($Na_{0.8}Li_yMe_{1-y}O_2$ vs. $Na_{0.67}MeO_2$). Ex situ solid-state NMR spectroscopy showed that Li ions are mostly located in the transition-metal layers as synthesized but tend to migrate to Na layers upon charge to higher voltages since octahedral and tetrahedral positions are available as stacking faults develop. However, the Li migration process is reversible.

Also on the topic of Li-rich layered sodium metal oxides, Komaba and co-workers recently reported a highly reversible capacity of 200 mAh g^{-1} for P2-$Na_{5/6}[Li_{1/4}Mn_{3/4}]O_2$ cycled at 1.5–4.4 V, which is higher than its theoretical capacity based on Mn^{3+}/Mn^{4+} redox. A long voltage plateau at 4.1 V at the first charge characterizes this system,[36] similar to layered lithium-rich oxides.[37,38] No transition to O2 or OP4 phases at the fully charged state occurs, similar to the P2-$Na_{0.8}[Li_{0.12}Ni_{0.22}Mn_{0.66}]O_2$ phase discussed above. Interestingly, superlattice peaks associated with Li/Mn ordering disappear when the cell is charged to 4.4 V, which indicates an in-plane cation rearrangement. As a consequence of similarities with lithium-rich Li_2MnO_3-based electrodes, (high capacities associated with high voltage plateaus and disappearing super-

structure by in-plane cation rearrangement), it is proposed that charge compensation in this material is fulfilled by partial removal of oxygen from the structure. This material shows high promise for Na ion battery applications because of its high specific capacity, moderate capacity retention, and also relatively high sodium content which is advantageous for use in a full Na ion cell.

Bruce and co-workers investigated P2-$Na_{0.67}Mn_{1-y}Mg_yO_2$ ($y = 0$, 0.05, 0.1, 0.2) made of earth-abundant elements.[39] Electrochemical studies demonstrated that substitution of Mn with Mg (up to 25%) enhances the capacity retention, decreases the polarization, and suppresses the phase transitions that pure P2-$Na_{0.67}MnO_2$ undergoes during the charge/discharge process. The effect of the cooling rate during synthesis on the crystal structure and electrochemical performance of the compounds was also examined. Both Mg substitution and slow cooling suppress the orthorhombic distortion by increasing the average oxidation state of Mn—or in other words, decreasing the concentration of Jahn—Teller-active Mn^{3+} ions—which leads to improved cyclability at the expense of a slight loss of capacity. P2-$Na_{0.67}Mn_{0.8}Mg_{0.2}O_2$ delivers an initial discharge capacity of 150 mAh g^{-1} between 1.5 and 4 V with an excellent retention of capacity of 96% over 25 cycles. On the other hand, Komaba and co-workers reported a surprisingly high discharge capacity for a similar composition, $Na_{0.67}Mg_{0.28}Mn_{0.72}O_2$, when charged to higher voltages.[40] This material delivers a discharge capacity of 220 mAh g^{-1} between 1.5 and 4.5 V, beyond the capacity adapted from the Mn^{3+}/Mn^{4+} redox reaction, although fading occurs on cycling. A large fraction of this reversible capacity is associated with a well-defined voltage plateau at 4.2 V (Figure 4). This anomalous reversible capacity is proposed to originate from activation of the redox reaction of the oxide ions by Mg ions, similar to the effect of lithium in Li-rich manganese oxides, or P2-$Na_{5/6}[Li_{1/4}Mn_{3/4}]O_2$ as discussed above. This is the first report of activation by Mg^{2+}. Although the problem of voltage fading in the Li- and Mn-rich analogues of these materials used in Li ion batteries has proven to be unsurmountable to date,[41] it remains an open question as to whether the different structural features of the sodium-based "high-voltage" layered oxides will be sufficient to overcome this issue. The concept shows promise for future explorations.

Achieving full capacity in sodium-deficient P2 phases in practical full-cell Na ion batteries requires sodium compensation by strategies such as predischarge with metallic sodium or the use of sacrificial salts. O3 phases, on the other hand, have the advantage of full sodium content. Johnson and co-workers have investigated the performance of a layered sodium metal oxide electrode in a full cell based on O3-$NaNi_{1/3}Fe_{1/3}Mn_{1/3}O_2$/hard carbon.[42] The capacity of the cell is limited due to irreversible processes associated with the carbon negative electrode that emerge from the formation of a solid electrolyte interphase (SEI) in the first cycle. Nevertheless, the cell demonstrates excellent stability and a smooth charge/discharge profile coupled with an impressive rate capability. The cell delivered a specific capacity of 100 mAh g^{-1} for 150 cycles in the voltage range of 1.5–4 V at a rate of 0.5 C. Ex situ X-ray diffraction analysis showed that the $R\bar{3}m$ structure of the positive electrode material was preserved after 123 cycles.

High-performance, low-cost O3 layered oxides are particularly desirable. Yamada and co-workers investigated the effect of Ni substitution on the electronic and electrochemical properties of O3-$NaFeO_2$.[43] Solid solutions of O3-$NaFeO_2$ and $NaNiO_2$ were formed over only a narrow compositional range ($0.5 \le y \le 0.7$ in $NaFe_{1-y}Ni_yO_2$). Phase separation in other compositions is attributed to large local lattice strain induced by substitution of spherical high-spin Fe^{3+} by anisotropic low-spin Ni^{3+} ions. The electrochemical performance of O3-$NaFe_{1-y}Ni_yO_2$ ($y = 0$, 0.5, 0.7) showed that substituting iron with nickel ions results in an enhanced discharge capacity and improved cyclability but at the expense of a decreased voltage of the cell (Figure 5). Ex situ X-ray diffraction revealed that sodium deintercalation from $Na_xFe_{0.3}Ni_{0.7}O_2$ progresses through a solid-solution process for

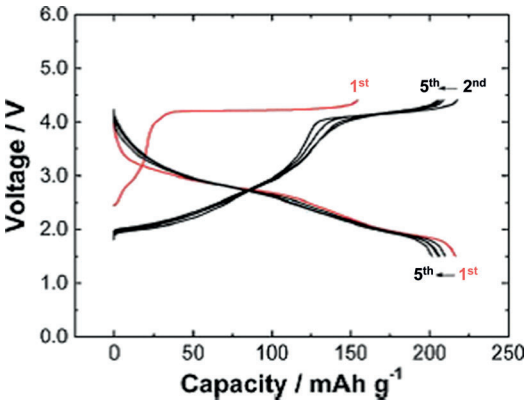

Figure 4. Galvanostatic charge/discharge curve of P2-$Na_{2/3}Mg_{0.28}Mn_{0.72}O_2$ in a Na cell cycled in the voltage range of 1.5–4.4 V at a rate of 10 mA g^{-1}. Reproduced from Ref. [40] with permission. Copyright 2014, The Royal Society of Chemistry.

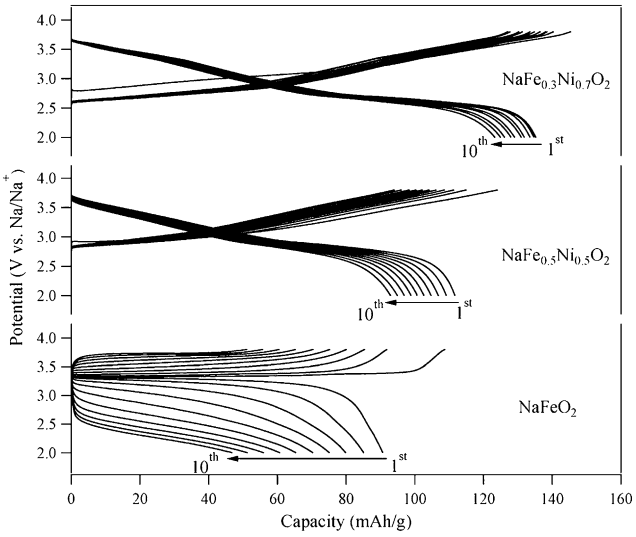

Figure 5. Galvanostatic charge/discharge curves of O3-$NaFe_{1-y}Ni_yO_2$ ($y = 0$, 0.5, 0.7) cycled in the voltage range of 2–3.8 V at a rate of 30 mA g^{-1}. Reproduced from Ref. [43] with permission. Copyright 2014, American Chemical Society.

most of the cycling range, in contrast to the two-phase process in Na_xFeO_2. Improved cycling stability in the Ni-substituted electrode materials is believed to be due to suppression of the phase separation in addition to decreasing formation of Jahn–Teller Fe^{4+} ions.

Despite the advantages that layered sodium transition metal oxides offer for electrochemical energy storage applications, their air sensitivity is a challenge. This is an important issue in terms of the reproducibility of results from research studies on these materials, in addition to concerns over storage and handling from a large-scale application point of view. It was reported long ago that water molecules can intercalate into P2-$Na_{2/3}[Co_xNi_{1/3-x}Mn_{2/3}]$ ($x = 1/6$, $1/3$), but not into its lithiated counterpart.[44] What differentiates sodium from the lithium metal oxide framework are the large empty prismatic sites and the large interslab space available in the P2 structure. On the other hand, no water intercalation was observed for P2-$Na_{2/3}[Ni_{1/3}Mn_{2/3}]O_2$ as claimed in the same report. In a more recent study, Passerini and co-workers investigated the correlation between the intercalation of water and the sodium content in the mixed P2/P3 structure $Na_xNi_{0.22}Co_{0.11}Mn_{0.66}O_2$.[45] The cells were charged to different voltages corresponding to specific sodium contents, disassembled, and exposed to air for analysis. XRD data of the cathodes suggest that water does not intercalate into this material until the sodium content decreases below a threshold amount. Below $x \approx 0.33$, intense $(00l)'$ peaks appear, indicative of a highly ordered hydrated phase with large interslab distances. In another study, Prakash and co-workers reported the structural instability of O3-$NaNi_{1/3}Mn_{1/3}Co_{1/3}O_2$ in an ambient atmosphere.[46] XRD analysis showed that as-prepared rhombohedral O3-$NaNi_{1/3}Mn_{1/3}Co_{1/3}O_2$ undergoes phase transitions to monoclinic O1 and then rhombohedral P3 phases when aged in air (Figure 6).

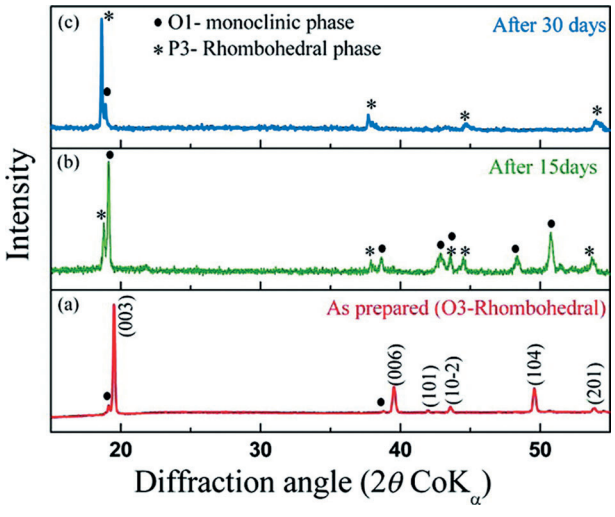

Figure 6. Powder X-ray diffractogram of $NaNi_{1/3}Mn_{1/3}Co_{1/3}O_2$ showing its structural instability on aging in air. a) Crystal structure of the as-prepared rhombohedral O3 phase. b) Monoclinic O1 phase after exposure to air for 15 days. c) Rhombohedral P3 phase after exposure to air for 30 days. Reproduced from Ref. [46] with permission. Copyright 2012, American Chemical Society.

We have recently demonstrated, through a deliberate study on the uptake of gases by P2 sodium-deficient phases such as $Na_xMn_{0.5}Fe_{0.5}O_2$, that the reactivity is much more complex than previously thought.[47]

3.2. Sodium "Polyanion" Electrochemistry

Polyanionic framework compounds based on phosphates, fluorophosphates, sulfates, and other new "polyanion" tetrahedral motifs of the type XO_4 or trigonal XO_3 combined with octahedral metal MO_6 (or other coordination centers) offer vast opportunities for developing novel cathode systems for Na ions. Diverse open-framework structures, the presence of low-energy Na^+ migration pathways, possibilities of tuning the operating voltage by modifying the local environments, and favorable structural energetics for a flat voltage response offer some crucial advantages. In addition, their robust covalent frameworks render them thermally stable and ensure impressive oxidative stability at high charging voltages. It is no surprise that in parallel to oxide materials, a plethora of polyanionic sodium compounds have been explored as cathode materials for secondary Na ion batteries. Some notable examples are discussed below.

3.2.1. Phosphates, Fluorophosphates, and Pyrophosphates

$NaFePO_4$, unlike its celebrated lithium analogue olivine-type $LiFePO_4$, crystallizes in the more thermodynamically stable maricite structure (Figure 7 a,b),[48] which has no free pathways for the diffusion of Na ions.[49,50] Electrochemically active olivine-type $NaFePO_4$ was prepared by low-temperature Li/Na exchange from $LiFePO_4$. The structural features are preserved in this process.[51] Its electrochemical profile (Figure 8 a) exhibits a distinct intermediate phase, $Na_{0.7}FePO_4$.[52] Despite calculations that suggest good ion mobility,[53] its electrochemical kinetics are very sluggish compared to $LiFePO_4$. This is in great part due to a much larger volume change between the reduced and oxidized phases. The excellent kinetics of the $LiFePO_4$ system have recently been attributed to the participation of a solid-solution phase which is accessed at relatively low overpotentials.[54,55] Such a metastable phase is unlikely for the Na ion analogue.

The more-promising NASICON compounds with open 3D frameworks, which are built-up of corner-sharing MO_6 and XO_4 polyhedra, possess large tunnels for the fast conduction of Na ions. These compounds were initially explored as solid electrolytes[6] and more recently as insertion materials. Amongst the various NASICON compounds, $Na_3V_2(PO_4)_3$ has emerged as an interesting candidate because of its impressive energy density (400 $Wh\,kg^{-1}$) and thermal stability in the charged state.[56] Its electrochemical profile exhibits two voltage plateaus at 3.4 V and 1.6 V, which correspond to the V^{3+}/V^{4+} and V^{2+}/V^{3+} redox couples, respectively. Only the higher voltage couple is suitable for a positive electrode. Owing to its poor electronic conductivity, researchers have struggled to achieve the theoretical specific capacity at practical current rates, but nanostructured design

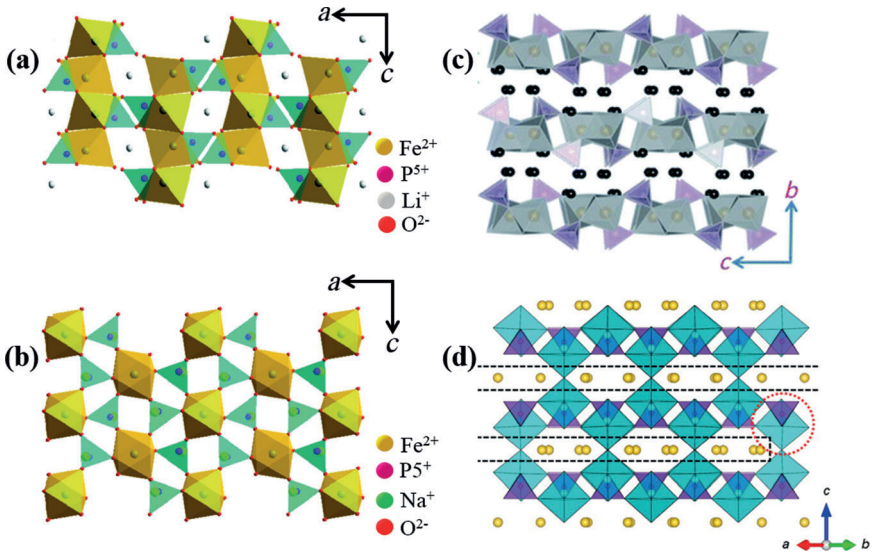

Figure 7. Structures of a) olivine $LiFePO_4$ and b) maricite $NaFePO_4$ in the 101 plane. Reproduced from Ref. [50] with permission. Copyright 2011, American Chemical Society. c) Fe and Na layers in the Na_2FePO_4F structure (FeO_6 octahedra are shown in gray, PO_4 tetrahedra are pink, and the black spheres denote Na). Adapted from Ref. [94] with permission. Copyright 2013, The Royal Society of Chemistry. d) Crystal structure of $Na_{1.5}VPO_{4.8}F_{0.7}$ with VO_5F/VO_4F_2 octahedra shown in cyan and yellow spheres representing the Na^+ ions. Reproduced from Ref. [62] with permission. Copyright 2013, American Chemical Society.

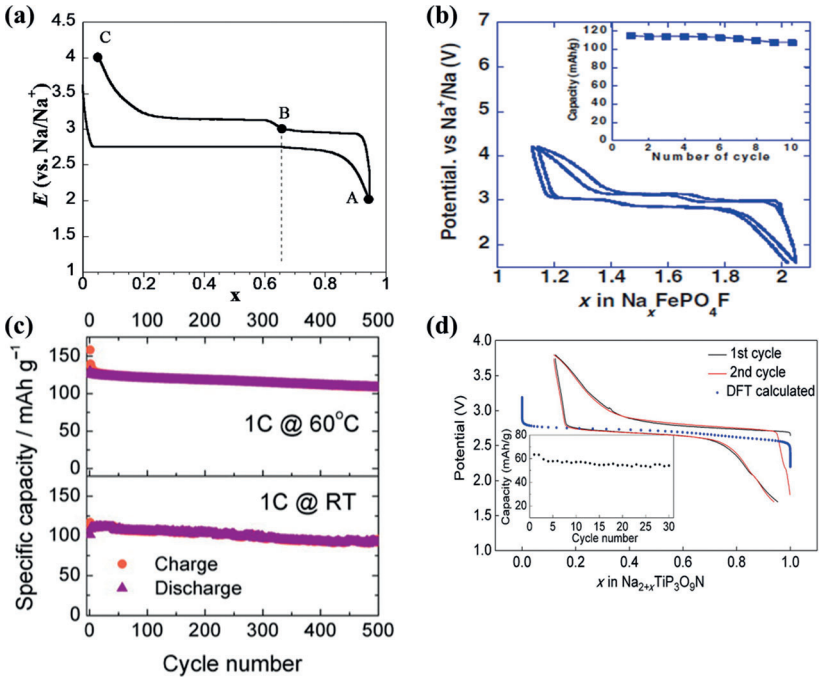

Figure 8. a) Typical electrochemical profile of olivine $FePO_4$ with and without intercalated sodium/ Reproduced from Ref. [48]. Copyright 2010, American Chemical Society. b) Electrochemical profile of Na_2FePO_4F cycled versus Na/Na^+ at a rate of C/15. Adapted from Ref. [63]. Copyright 2009, The Electrochemical Society. c) Electrochemical cyclability of the $Na_{1.5}VPO_{4.8}F_{0.7}$ electrode at 25 °C (bottom) and 60 °C (top) at 1 C rate between 2.0–4.7 V. Reproduced from Ref. [62]. Copyright 2013, American Chemical Society. d) C/20 charge/discharge curve of $Na_3TiP_3O_9N$ against Na/Na^+. The blue dotted line shows the DFT calculated voltage profile. Reproduced with permission from Ref. [76]. Copyright 2014, American Chemical Society.

has come to the rescue. Impressive cycling stability and rate capability have been demonstrated in two separate reports by utilizing carbon-coated nanoparticles embedded in a porous carbon matrix[57] and a carbon nanofiber with encapsulated nanoparticles produced by electrospinning.[58]

The inclusion of highly electronegative fluorine atoms in the covalent polyanionic framework is known to boost the voltage of the active redox couple. One example is the fluorine-containing NASICON analogue $Na_3V_2(PO_4)_2F_3$,[59] which is promising because of its high average voltage of 3.9 V and theoretically predicted single-phase behavior with negligible volume change (2%).[60] Other examples include Na_2FePO_4F,[61] and $Na_{1.5}VPO_{4.8}F_{0.7}$.[62] The former consists of a layer-like two-dimensional framework of $Fe_2O_7F_2$ bioctahedra connected by PO_4 tetrahedra (Figure 7c), which house two Na^+ ions in the interlayer space. This material was first reported by our group in 2007,[61] and has been the focus of several excellent studies on Na ion cells since then.[63,64] Retention of one of the Na^+ ions in the structure on oxidation props open the layers, thereby resulting in a small volume change (3.7%).[61] The electrochemical profile of Na_2FePO_4F is shown in Figure 8b. Both the charge and discharge profiles exhibit two two-phase plateaus, centered at 2.90 V and 3.05 V versus Na/Na^+, and 80% of the 120 mAh g^{-1} theoretical capacity was sustained after 10 cycles. A combination of Mössbauer and XRD studies revealed a single line-phase composition—$Na_{1.5}FePO_4F$—that adopts $Fe^{2+/3+}$ ordering in the form of paired dimers.[65] This localizes the electron-charge carriers, and so despite the excellent mobility of the Na ions, the electrochemical kinetics are not as favorable as in $Na_{1.5}VPO_{4.8}F_{0.7}$, which also exhibits a layered structure. The latter compound is constructed of corner-sharing VO_5F/VO_4F_2 octahedra (V^{4+} and V^{3+}) and PO_4 tetrahedra (Figure 7d).[62] Park et al. demonstrated the exceptional cycling performance of this material, with 95% and 84% capacity retention after 100 and 500 cycles, respectively, at a rate of 1 C (Figure 8c) and negligible overpotential throughout the charge/discharge process. Such outstanding electrochemical performance is attributed to the small volume change on Na ion cycling, fast Na ion diffusion ($E_a \approx 0.35$ eV) in the *ab*

plane of the $P4_2/mnm$ structure, and lack of ordered compositions within the redox window.

Inspired by the success of $Li_2MP_2O_7$ compounds, the Yamada research group has developed a series of sodium analogues: triclinic ($P\bar{1}$) $Na_2FeP_2O_7$,[66] ($P1$) $Na_2MnP_2O_7$[67] with 3D Na ion channels, and layered orthorhombic $Na_2CoP_2O_7$,[68] with 2D channels for Na^+ mobility. All three demonstrate reversible Na ion storage with a capacity of approximately 80 mAh g^{-1} at an average voltage of 3 V for the Fe and Co compounds and about 3.6 V for the Mn compound. This is one of the highest reported Mn^{2+}/Mn^{3+} redox couples for a sodium pyrophosphate; the electrochemical activity in comparison to the inactive manganese phosphates such as $LiMnPO_4$ is noteworthy.

3.2.2. *Fluorosulfates and Sulfates*

Studies on fluorosulfates with a structure related to the open framework of the mineral tavorite[69] reveal interesting comparisons to their lithium analogues. They offer advantages over their phosphate cousins because of a greater inductive effect that raises the potential by as much as 0.8 V. Their moisture sensitivity demands synthesis in non-aqueous media, which resulted in the discovery of a corner-shared $NaFeSO_4F$ framework.[70,71] Atomistic modeling studies of the energy barrier to Na hopping in this material revealed that it is effectively a 1D ion conductor with an activation barrier of 0.6 eV,[72] in sharp contrast to $LiFeSO_4F$ which exhibits 3D Li^+ ion hopping with a barrier as low as 0.35 eV as a consequence of its slightly different structure. The limited ion mobility of $NaFeSO_4F$, along with a large volume change on redox, results in much poorer electrochemical properties.

Sulfates have been explored more recently. Polymorphs of the bloedite-type $Na_2M(SO_4)_2{\cdot}4H_2O$ (M = Mg, Fe, Co, Ni),[73] and kröhnkite-type $Na_2Fe(SO_4)_2{\cdot}2H_2O$[74] have been synthesized and explored electrochemically. Both bloedite-type $Na_2Fe(SO_4)_2{\cdot}4H_2O$ and its dehydrated derivative show electrochemical activity at approximately 3.3 V versus Na, with the former losing structural water simultaneously with desodiation, which results in amorphization on charging. In contrast, kröhnkite-type $Na_2Fe(SO_4)_2{\cdot}2H_2O$ displays a Fe^{2+}/Fe^{3+} redox couple at about 3.25 V with good structural reversibility. Discovery of a sulfate with a new composition and structure based on the alluaudite-type framework, $Na_2Fe_2(SO_4)_3$, represents a leap forward.[75] It has registered the highest ever Fe^{3+}/Fe^{2+} redox potential at 3.8 V versus Na along with fast kinetics. A unique structure among iron sulfates that exhibits edge-shared FeO_6 octahedra (Figure 9a, unlike the corner-shared NASICON analogues) accounts for the remarkably high redox potential of this compound. A reversible capacity of 102 mAh g^{-1}—85% of the theoretical value—is delivered. A sloping voltage profile over the entire range of Na composition (Figure 9b) indicates a single-phase reaction mechanism as verified by in situ XRD studies. A strikingly small volume change of 1.6% upon de/sodiation accounts for the high reversibility and impressive rate performance of the material.

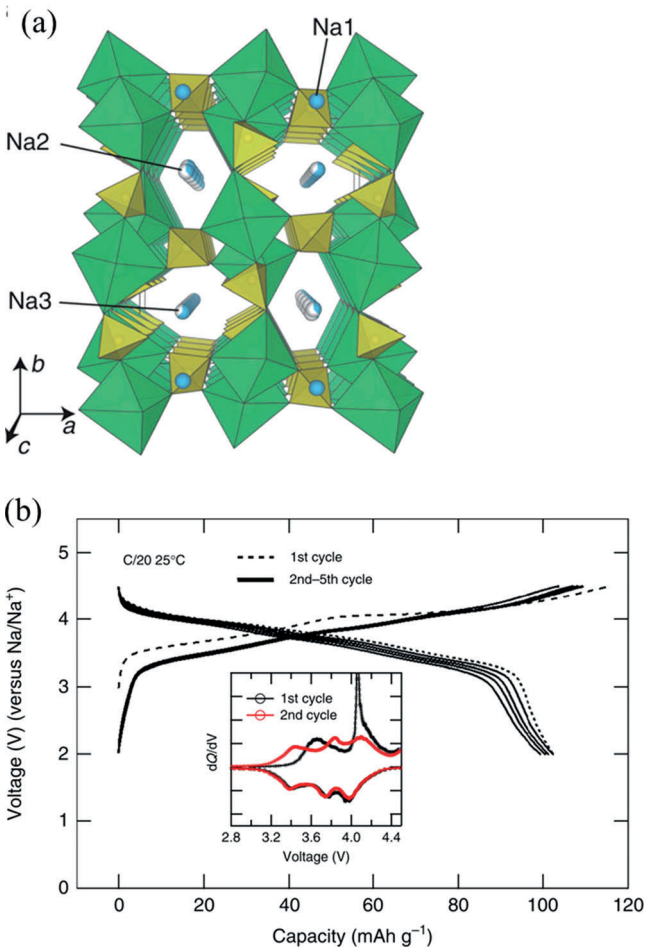

Figure 9. a) The structure of $Na_2Fe_2(SO_4)_3$ projected along the c axis. Green octahedra, yellow octahedra, and blue spheres denote FeO_6, SO_4, and Na, respectively. b) Galvanostatic discharge/charge profile of $Na_{2-x}Fe_2(SO_4)_3$ cycled at a C/20 rate against Na in a 2–4.5 V window. The inset shows the differential galvanostatic profile with two distinctive peaks during the first charge. Adapted from Ref. [75] with permission. Copyright 2014, Nature Publishing Group.

3.2.3. *New Polyanion Materials*

An interesting new addition to the polyanionic cathode family is the nitridophosphate $Na_3TiP_3O_9N$. This compound is created by synthesis in flowing ammonia, which results in partial substitution of oxygen by nitrogen in the phosphate groups.[76] This material, effectively $Na_3Ti_2(PO_4)_2(PO_3N)$, displays a high average voltage of 2.7 V against Na (0.6 V higher than the equivalent Ti^{4+}/Ti^{3+} redox couple of the parent NASICON-type $Na_3Ti_2(PO_4)_3$ cathode) because of the inductive effect of the N^{3-} ion in the $[PO_3N]$ groups. Electrochemical Na de/intercalation occurs through a solid-solution route with an extremely low volume change for extraction of the Na ions (<1%). The electrochemical voltage profile overlaid with that calculated from DFT is shown in Figure 8d. Even though the capacity of the Ti compound is limited (74 mAh g^{-1}), the presence of two cyclable Na ions in the lattice suggests a significant increase

in the capacity of a possible analogue in which multiple redox processes can be accessed.

Another new class of polyanionic compounds, the carbonophosphates, has recently been introduced as cathode materials by the Ceder research group.[77] Ab initio computational modeling revealed that the $Na_3MCO_3PO_4$ (M = Mn, Fe) structure is suitable for more than two redox processes, but at slow rates. The synthesis and Na ion intercalation properties of the Fe analogue have also been demonstrated very recently.[78] In situ and ex situ X-ray absorption near-edge spectroscopy (XANES) have been applied, thereby uncovering the activity of both the Fe^{2+}/Fe^{3+} and Fe^{3+}/Fe^{4+} redox couples during discharge and charge processes.

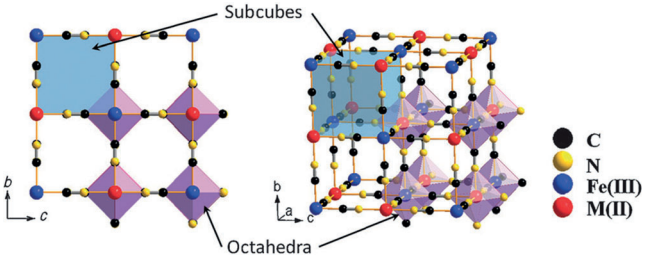

Figure 10. Framework of Prussian blue analogues showing the double perovskite lattice of M^{II} and Fe^{III}, and ordered arrangement of the CN^- linkers. Reproduced from ref. [80] with permission. Copyright 2012, Royal Society of Chemistry.

3.3. Prussian Blue Cathodes

In recognition that lattice volume expansion/contraction on redox is more problematic for the larger Na^+ ion than Li^+, so-called Prussian-blue analogues (PBAs) have been investigated as intriguing alternative cathode materials to the layered oxide and polyanion structures. Alkali metal de/insertion is less hindered in the relatively open framework PBA structure, which allows for more flexibility in cation accommodation and extraction on redox. The prototype ideal Prussian blue, $(K[Fe^{III}Fe^{II}(CN)_6]y{\cdot}H_2O$, $y \approx 1$–5) has a cubic structure consisting of Fe^{II} and Fe^{III} ions sitting on alternate corners of corner-shared iron octahedra bridged by cyano $(C{\equiv}N)^-$ ligands.[79] The cyano ligands link the active metal redox centers together to form cagelike structures. This open-framework contains channels (3.2 Å) and interstitial sites (4.6 Å) that enable rapid solid-state diffusion of a wide variety of ions, including Na^+. Although it is called "soluble" Prussian blue (SPB), it is actually highly insoluble.

Once the domain of the coordination chemist of the last century, PBAs have generated enormous interest for both aqueous (where the voltage is limited to 1.5 V)[13] and non-aqueous batteries in the last three years. The latter are reviewed here. PBAs can be more generally described as $Na_{2-x}M_A[M_B(CN)_6]_{1-y\square y}{\cdot}z\,H_2O$. Many different transition metals M_A and M_B can be accommodated, and hexacyanometallate vacancies ($\square y$) in the $[M_B(CN)_6]^{4-}$ moities often exist. In so-called insoluble Prussian blue, $Fe_4[FeCN)_6]_3$, for example, one-quarter of the $[Fe^{II}(CN)_6]^{4-}$ sites are occupied by water. Crystal-field-derived energetic factors drive directional alignment of the CN^- ions within the double-perovskite $M_A[M_B(CN)_6]$ cage, and the formation of low-spin M_BC_6 and high-spin M_AN_6 metal octahedra. The carbon atom of the CN^- is connected to M_B, and the N atom of the CN^- is bonded to M_A. These materials are capable—in principle—of reversible extraction of two Na ions per formula unit at high rates with good cycle life, if both metal centers are M^{II}. The structure of a typical PBA is shown in Figure 10.

As a consequence of their low cost and facile synthesis, the hexacyanoferrates (M_B = Fe) are the most popular PBAs. Goodenough et al. introduced the $KMFe(CN)_6$ family (M^{II} = Mn, F, Co, Ni, Zn) as non-aqueous sodium ion cathodes in 2012.[80] The Fe^{II} compound exhibits a capacity of approximately 100 $mAh\,g^{-1}$ in a Na ion cell, with two high-potential plateaus at 3.5 V and 2.8 V. The higher potential corresponds to the high-spin Fe^{III}/Fe^{II} couple bonding to N, and the lower voltage to the low-spin Fe^{III}/Fe^{II} couple bonding to C. A capacity of about 60 $mAh\,g^{-1}$, close to the theoretical value, was reported for $Na_2Zn_3[Fe^{II}(CN)_6]_2{\cdot}x\,H_2O$.[81] Thin films of hexacyanoferrates have been explored for their high rate capabilities[82] and mesoporous modifications.[83] Frameworks where $M_A = M_B$ = Fe or Mn are particularly attractive for large applications where cost is a factor. Sodium manganese hexacyanoferrate ($Na_{2-x}MnFe(CN)_6$) with a high sodium concentration was reported to be a promising cathode material because of its high capacity (134 $mAh\,g^{-1}$) and voltage resulting from the Mn^{III}/Mn^{II} redox couple.[84] However, only 120 $mAh\,g^{-1}$ was maintained over 30 cycles. The material "Berlin green" $[Fe^{III}Fe^{III}(CN)_6]$ was reported to undergo sodium insertion with a reversible capacity of 120 $mAh\,g^{-1}$ and 87% capacity retention over 500 cycles.[85] This was claimed to be achieved by controlling the purity and crystallinity of the PBA structure.

A more desirable tactic is to access a reduced variation of the PBA compositions—"Prussian white", which is mostly Fe^{II}, counterbalanced by a high sodium content in the $Na_{2-x}Fe[Fe(CN)_6]$ framework. This allows for a Na-free anode to be used practically, similar to the layered oxide and polyanion materials. A variable sodium composition $Na_{2-x}Fe[Fe(CN)_6]$ was prepared by a facile synthetic procedure by using $Na_4[Fe(CN)_6]$ as the precursor.[86] Rapid precipitation from the acidic medium gives low-quality material (see Figure 11) where a high level of very disordered $[Fe(CN)_6]$ vacancies are proposed to exist (presumably filled with water), whereas the slower-growing process produces high-quality (HQ)-NaFe nanocubes with a more crystalline structure. The positive effect of the low water content and small number of $[Fe(CN)_6]$ vacancies on the electrochemical performance of HQ-NaFe is shown in Figure 11c,d. The optimized material exhibits a Coulombic efficiency of about 98%.

The importance of minimizing the fraction of vacancy sites and maximizing M^{II} content is nicely demonstrated by the very recent report of $Na_2Mn^{II}[Mn^{II}(CN)_6]$ by the Cui research group.[87] They were able to crystallize 100 nm cubes of almost perfectly stoichiometric $Na_{1.96}Mn[Mn(CN)_6]_{0.99}\square_{0.01}{\cdot}2\,H_2O$ by using a large excess of sodium. A surprisingly high reversible capacity of 209 $mAh\,g^{-1}$ was achieved in a propylene carbonate electrolyte. The additional

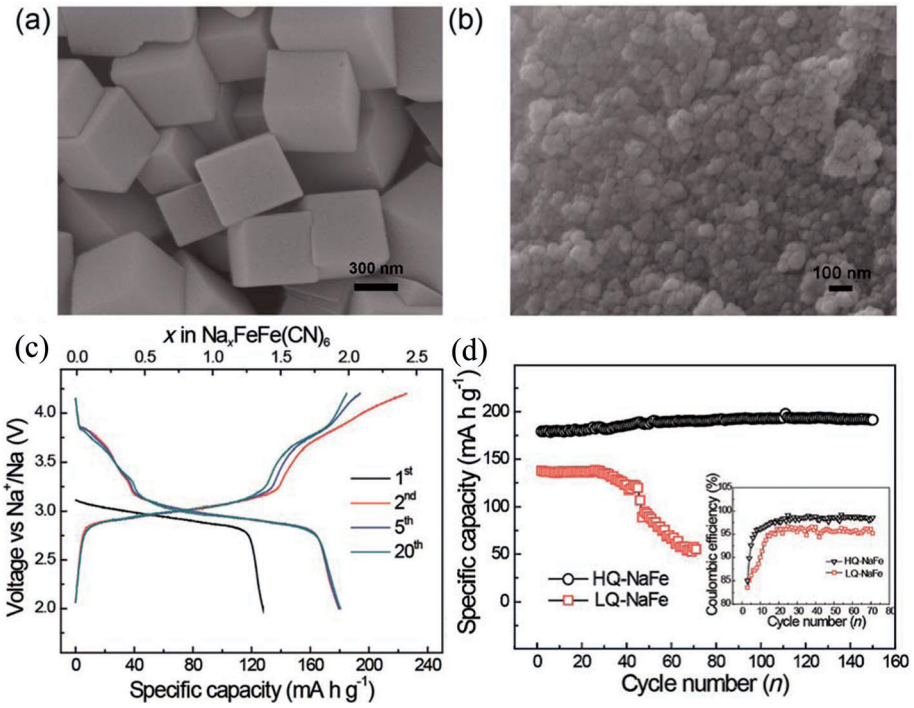

Figure 11. SEM images of a) high-quality (HQ) nanocubes of $Na_{0.61}Fe[Fe(CN)_6]_{0.94}\square_{0.06}$ and b) low-quality (LQ) $Na_{0.13}Fe[Fe(CN)_6]_{0.68}\square_{0.32}$. c) Galvanostatic discharge/charge profiles of HQ-NaFe over 20 cycles. d) Comparison of the cycling performance of HQ-NaFe and LQ-NaFe. Adapted from Ref. [86] with permission. Copyright 2014, Royal Society of Chemistry.

capacity above that expected for extraction of two Na^+ ions from a vacancy-free material ($170\,mAh\,g^{-1}$) arises from reduction to $Na_3Mn^{II}[Mn^{I}(CN)_6]$ on initial discharge, which allows for full cycling of 3 Na^+ ions.

4. Computational Studies of Na Ion Mobility

Synergistic experimental and computational approaches to materials development are rapidly becoming the norm to accelerate materials discovery and characterization, and to gain fundamental insight into structure–property relationships.

A recent comprehensive review has aptly summarized the power of computational approaches in gaining a fundamental understanding of the atomic-scale properties of positive electrode materials for LIBs and NIBs.[88] Two main types of computational techniques are typically adopted: electronic structure investigations based on DFT and Hartree–Fock methods, and methods based on interatomic potentials. DFT methods have been applied to oxide insertion materials. The difference between Na and Li ions in a variety of compounds is highlighted with respect to voltage, phase stability, and activation energy for ion mobility.[89] The authors demonstrate that the generally lower calculated voltages for Na compounds are due to the smaller energy gain obtained from inserting Na into a host structure relative to that of Li. The differences, typically between 0.18 and 0.57 V, may be especially advantageous for the design of negative electrode materials for sodium batteries. Their calculations also show that Na^+ migration barriers may be lower than the corresponding Li^+ migration barriers in layered oxides. DFT studies on $Na_{0.44}MnO_2$,[90] P2-$Na_{2/3}[Ni_{1/3}Mn_{2/3}]O_2$,[91] and Na_xCoO_2[92] illustrate the importance of structure. The study by Lee et al. predicted higher Na^+ diffusivity for the P2-type compound than the corresponding O3-type Li compound.[91] In a very recent article involving an ab initio computational based study of P2- and O3-Na_xCoO_2, Mo et al. gained comprehensive insight into concentration-dependent Na^+ diffusivity in those structures (Figure 12).[93] Both the P2 and O3 structures show good Na^+ mobility over a wide range of Na concentrations, although P2 outperforms O3 except at the highest concentration.

Tripathi et al. used atomistic potential based methods to explore Na^+ migration in the polyanion materials olivine $NaMPO_4$ (M = Mn, Fe) and Na_2FePO_4F, thereby confirming the 1D nature of Na^+ mobility in the olivine and high Na^+ mobility through a 2D network in the *ac* plane of layered Na_2FePO_4F.[94] Atomic potential based simulation studies revealed the stability of the $Na_2MP_2O_7$ (M = Mn, Fe) framework towards oxygen evolution, along with a curved path for

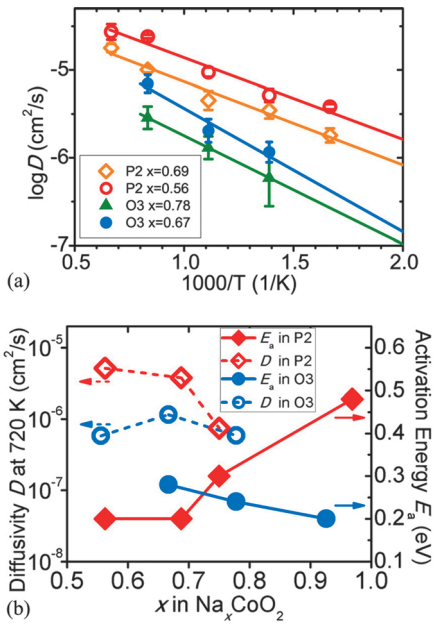

Figure 12. a) Arrhenius plot of Na diffusivity in P2 and O3 Na_xCoO_2, and b) Activation energy (E_a) and diffusivity at 720 K as a function of Na concentration *x* in P2- and O3-Na_xCoO_2 obtained by first principles calculations. Adapted from Ref. [93]. Copyright 2014, American Chemical Society.

3D Na^+ diffusion parallel to the *a*, *b*, and *c* crystallographic directions with a low activation energy ($\approx$0.5 eV).[95] Ab initio calculations on the reversible and high rate cathode host $Na_2Fe_2(SO_4)_3$ (see Section 3.2) gave quantitative insights into the fast Na^+ dynamics in its open framework structure.[75] A liquid-like activation energy value of 0.14 eV was calculated for defect diffusion along the Na3 channels of the *C*2/*c* structure. Based on this study, 1D Na^+ conduction was postulated along the *c* axis for both the Na2 and Na3 sites, whereas Na1 can be extracted through the Na3 site. Thus, all the Na ions are extractable, with no limit on achieving the theoretical specific capacity.

Computational approaches underline the importance of three crucial considerations in NIB cathode materials design: 1) a small volume difference (<5%) between the end members for Na^+ de/intercalation, 2) a low activation energy for Na^+ transport, and 3) preferably complete absence of antisite defects for good capacity retention and rate capability. The different interaction of the larger Na^+ ions (compared to Li^+) with liquid electrolytes—including ion mobility in the electrolyte and the thermodynamics of desolvation at the cathode interface—is also of importance and relevant to computational studies, although this topic is beyond the scope of this Review.

5. Anode Materials

Sodium metal anodes are commonly used on the laboratory scale to evaluate the performance of cathode materials. However, the formation of dendrites and the safety issues related to sodium metal currently prevent its use as a negative electrode for commercial applications. Thus, the success of Na ion batteries is strongly dependent on the development of safe and efficient anode materials.

5.1. Carbons

Sodium atoms do not intercalate significantly in graphitic carbons, which are the basis of the most common negative electrode in Li ion batteries.[96–98] As a result, hard (disordered) carbons—for example, prepared by the pyrolysis of sucrose—are the most studied negative electrode materials for Na ion batteries. They achieve reversible capacities up to 300 mAh g^{-1}.[99–101] The electrochemical potential of Na insertion into hard carbon is close to that of the metal itself, which indicates that there is very little carbon-to-sodium charge transfer. This is a signature of a mechanism whereby Na ions fill the porosity generated by the disordered hard carbon layers rather than intercalate between graphitic sheets.[98] The good performance of hard carbon as a negative material for Na ion batteries was recently demonstrated in full cells with O3-$NaMn_{0.5}Ni_{0.5}O_2$ as the positive electrode.[99] Despite some electrolyte decomposition, over 70% of the initial capacity is maintained after 50 cycles at moderate current density, and similar results are obtained at high current density (300 mA g^{-1}(carbon)).[102] Operating hard carbon anodes at a high current density and/or high depth of discharge represents a safety hazard, however, since the insertion potential is very close to the sodium plating potential. A porous hard carbon prepared based on a silica templating approach reported by Wenzel et al. shows a possible solution.[103] The high porosity and advanced microstructure enhanced the high rate capability, thereby resulting in a capacity of 180 mAh g^{-1} for the first cycle at a rate of C/5. This carbon outperformed several other industrial carbons.

Very recently, the insertion of sodium in expanded graphite was reported.[104,105] The spacing of the graphene layers strongly influences the reversible capacity. It increases from 25 mAh g^{-1} in graphite (d = 3.4 Å) to 136 mAh g^{-1}[104] or 174 mAh g^{-1}[105] in highly reduced graphene oxide (d = 3.7 Å), reaching 280 mAh g^{-1} at the optimal spacing of 4.3 Å.[104] The optimized material exhibits a stable reversible capacity of about 280 mAh g^{-1} at current densities of 20 mA g^{-1}(carbon), dropping to 180 mAh g^{-1} when the rate is increased to 100 mA g^{-1} (Figure 13). The capacity retention is more than

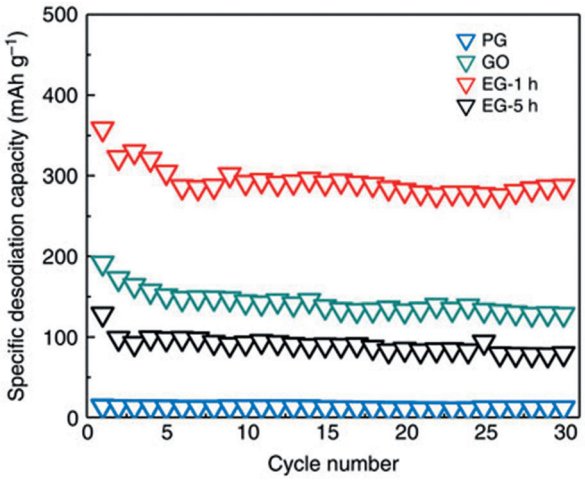

Figure 13. Short-term cycling stability test for graphite (PG, d = 3.4 Å), graphene oxide (GO, d = 6.1 Å), reduced graphene oxide (EG-1h, d = 4.3 Å), and reduced graphene oxide (EG-5h, d = 3.7 Å) at a current density of 20 mA g^{-1}. Reproduced from Ref. [104] with permission. Copyright 2014, Nature Publishing Group.

70% after 2000 cycles, which suggests that the expanded graphite negative electrodes have very encouraging aging properties. The insertion potential of these materials is a sloping curve from 1.5 V to 0 V with more than 80% of the capacity under 1 V. The higher voltage compared to hard carbon increases the safety at the expense of the energy density.

5.2. Low Potential Transition-Metal Oxides and Phosphates

Anodes based on the insertion of sodium into transition-metal oxides are of particular interest, where benefits arise from good safety features and high volumetric energy densities. Sodium insertion into NASICON-type $NaTi_2(PO_4)_3$ at 2.1 V was reported by Park et al. to undergo a two-phase mechanism.[106] The observed capacities for $NaTi_2(PO_4)_3$ in

both non-aqueous and aqueous electrolytes correspond to over 90% of the theoretical capacity of 133 mAh g^{-1}. The polarization observed in the aqueous electrolyte on cycling was substantially smaller as a result of its lower impedance and viscosity. The Na^+ insertion/extraction potential is located at the lower limit of the electrochemical stability window of the aqueous Na_2SO_4 electrolyte, which makes $NaTi_2(PO_4)_3$ an attractive negative electrode for aqueous sodium ion batteries.[13]

Titanates and vanadates usually exhibit good stability at low voltage, that is, resistance against a conversion mechanism. Vanadium layered oxides such as O3-$NaVO_2$,[4,107] and P2-$Na_{0.7}VO_2$,[108] show highly reversible sodium intercalation associated with complex structural evolution as elucidated by Delmas and co-workers, but the voltages ranging from 2.5 V to 1.5 V are too high for a practical anode material. Most of the current research interest focuses on titanates, which generally present acceptable voltages but poor electronic conductivity that hinders bulk storage of sodium. Sodium intercalation into amorphous TiO_2 nanotubes shows that their size is critical to obtaining significant Na intercalation.[109] The improved properties of larger tubes (inner diameter >80 nm, wall thickness >15 nm) was attributed to a larger number of Na^+ charge carriers because of the greater volume of electrolyte contained within the tube. $Na_2Ti_3O_7$ exhibits a particularly low desirable potential.[110] The insertion of two additional sodium atoms (180 mAh g^{-1}) occurs at a reversible plateau around 0.3 V versus Na/Na^+ (Figure 14). However, to achieve this capacity, a slow cycling rate (C/25) and a composite electrode with 30% carbon black are necessary. In addition to decreasing the energy density, carbon black is responsible for the large irreversible capacity which is of the same order of magnitude as the reversible capacity observed on the first cycle. The rate capability has been significantly improved by reduction of the particle size by either hydrothermal synthesis[111] to obtain 8 nm particles capable of reversible capacities up to 110 mAh g^{-1} at 4 C, or high-energy ball milling[112] to reduce the particles down to 100 nm and achieve 75 mAh g^{-1} at 5 C. In both cases the capacity retention is improved at higher rates, thus suggesting parasitic reactions because of the large surface area. Approaches to create improved architectures which have been reported for the lithium-insertion anode material, $TiNb_2O_7$,[113] may prove beneficial for its application in Na ion batteries.

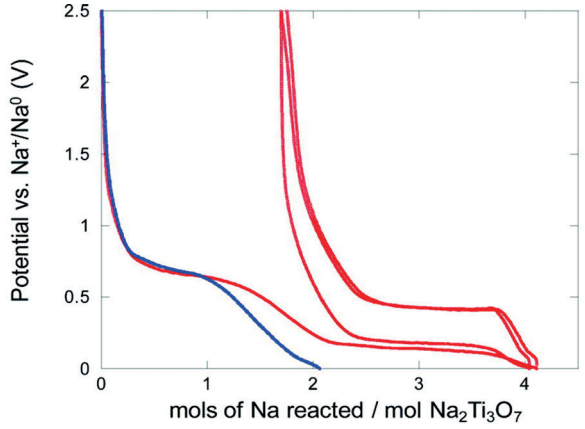

Figure 14. Voltage versus composition profile for the electrochemical reduction of a blank electrode containing only carbon black (blue curve) and a composite electrode containing $Na_2Ti_3O_7$ and 30% carbon black (red curve), where the reversible insertion of ca. 2 mol of sodium ions per mol $Na_2Ti_3O_7$ is observed. Reproduced from Ref. [110] with permission. Copyright 2011, American Chemical Society.

The superior capabilities of cathodes based on the P2 layered oxide led to the investigation of the same structure for negative electrode applications. Thus, $Na_{0.66}Li_{0.22}Ti_{0.78}O_2$,[114] with lithium in the transition-metal site, shows a reversible capacity of approximately 120 mAh g^{-1} at C/10 with an average voltage of 0.7 V versus Na/Na^+. This material exhibits good rate capability with 75 mAh g^{-1} at 1 C and 75% capacity retention after 1200 cycles. The good performance is attributed to the very small volume change (0.8%) upon sodium insertion. To increase the electronic conductivity of the layered titanium oxides and achieve efficient bulk storage of sodium, Fielden and Obrovac used Ni^{2+} rather than Li^+ to substitute for titanium in the structure.[115] By using this strategy they reported a reversible capacity of 110 mAh g^{-1} at a current rate of C/10 with a relatively flat potential around 0.7 V versus Na by using a composite electrode based on $Na_{0.6}Ni_{0.3}Ti_{0.7}O_2$ with only 10% carbon, which significantly improved the energy density compared to other titanates. The rate capability is poor, however, probably due to the large crystallite size (10 μm).

5.3. *Alloys*

As noted by Chevrier and Ceder,[116] much less research has been carried out on sodium alloy materials as negative electrodes for sodium ion batteries than for their lithium counterparts. Alloys have very high energy densities and low redox potentials, two highly desirable properties. The potentials for these reactions have been predicted,[116] and show promise. Silicon and germanium, the two most promising anode materials for Li ion batteries, do not intercalate sodium at room temperature; lead and bismuth achieve initial sodiation close to the theoretical values but present very poor cyclability[117,118] as expected because of their volume expansion of 250% and 365%, respectively. The strain caused by the large volume expansion upon insertion is problematic, even with less than full discharge. Careful design of the microstructure of the electrode is thus required, which has an impact on both the energy density and cost of manufacture. These issues have thus far inhibited the development of silicon anodes for lithium batteries, and the larger size of sodium with respect to lithium makes the design of such anodes for sodium ion batteries even more challenging.[119]

With an average voltage of 0.3 V versus Na and a theoretical capacity of 790 mAh g^{-1}, tin is a more promising candidate. Despite a volume expansion of 420%, composite electrodes of tin powder with a polyacrylate binder show a reversible capacity of 500 mAh g^{-1} over 20 cycles at a slow cycling rate.[117] Wang et al. used in situ transmission electron microscopy to verify that the Sn particles were able to accommodate the volume increase without cracking.[120] Careful analysis by in situ techniques revealed that the intercalation mechanism is dependent on the physical form

of the anode: amorphous/nanocrystalline phases are reported in the case of powders,[120,121] whereas foils tend to show much higher crystallinity.[122] In both case, kinetic effects are predominant and prevent the formation of the thermodynamically stable phases present in the Na-Sn phase diagram.

On a positive note, a large reversible capacity of 600 mAh g^{-1} over 160 cycles at a rate of C/10 with an average voltage of 0.8 V versus Na was reported for microcrystalline antimony.[123] The rate capability of this material is excellent, showing a reversible capacity of 500 mAh g^{-1} at a rate of 4 C. The composite electrode formulation—a mixture of carbon black and vapor-ground carbon fibers as the conductive additive (15%) and carboxymethyl cellulose as the binder (15%)—is partly responsible. It is interesting to note that the sodium cells perform better than their lithium counterparts. A possible explanation resides in the fact that, in contrast to lithium, sodium insertion in antimony generates an amorphous intermediate phase that is believed to release part of the strain associated with the intercalation process.

The insertion of sodium into amorphous phosphorus[124] achieves a remarkable capacity of 1500 mAh g^{-1} during first cycles at C/10, with an average potential of 0.6 V versus Na. About 1000 mAh g^{-1} is retained after 80 cycles. A decrease in the reversible capacity is observed at higher rates, with "only" 1000 mAh g^{-1} available at 1 C. The promising electrochemical properties can be attributed in large part to the high-energy milling of red phosphorus (70%) and super P carbon (30%) that results in an amorphous composite. The insertion of sodium into crystalline phosphorus yields a much smaller capacity, thus emphasizing the importance of the amorphous phase to release the strain arising from intercalation.

In all the studies showing good cyclability,[117,123,124] the addition of fluorinated ethylene carbonate (FEC) was the key to greatly enhanced capacity retention. In these systems, where "fresh" surface is constantly exposed to the electrolyte by electrochemical grinding, the passivation of the anode–electrolyte interphase is of the upmost importance. It is fortunate that FEC, initially reported as an additive for hard carbon, works well with so many different systems.

6. Electrolytes

The interface of the electrolyte with both the positive and the negative electrodes means its chemical stability requirements considerably limit the usable scope of material. Chemical compatibility is ensured through the formation of passivation layers, referred to as the solid electrolyte interphase (SEI). The formation and physical properties of those protective layers depend on the nature of the electrode (especially the negative), thus implying that the study of electrolytes is not easily decoupled from the electrodes. For sodium ion batteries, since there is no widely accepted negative electrode, systematic electrolyte studies are relatively scarce. In addition to providing a stable interface, an electrolyte must achieve good ionic conductivity. This parameter is mostly affected by the concentration of the charge carrier (solubility of the salt), the ionic mobility (viscosity of the media), and the ionic dissociation of the salt (dielectric constant of the media).

The electrolytes of interest for room-temperature Na ion insertion batteries can be classified into 1) non-aqueous electrolytes consisting of a sodium salt solubilized in an organic solvent and 2) ionic liquids (ILs) consisting of an organic salt (R^+X^-) doped with a fraction of the sodium salt equivalent (Na^+X^-). Despite significant progress in Na^+ solid electrolytes, which show possible applications at room temperature,[125] their conductivities are still 1–2 orders of magnitude lower at room temperature than the more traditional liquid electrolytes at present, thus leaving much scope for further development.

6.1. Non-Aqueous Electrolytes

All current non-aqueous electrolytes for Na ion batteries are based on carbonate solvents, such as ethylene carbonate (EC) and propylene carbonate (PC) because of their very high dielectric constants, large electrochemical windows, and low volatilities. Of the sodium salts studied—sodium bis(trifluoromethane)sulfonimide (NaTFSI), sodium triflate (NaOTf), sodium perchlorate ($NaClO_4$), and sodium hexafluorophosphate ($NaPF_6$)—the latter two are optimum. As expected from carbonate solvents, their oxidative stability is good, and compatibility with the positive electrode is not a major concern. This is illustrated in the case of $NaCrO_2$, where Coulombic efficiencies greater than 99.70% were measured after 50 cycles in symmetric cells ($Na_{rich}CrO_2$/$Na_{poor}CrO_2$) with either NaTFSI or $NaPF_6$ in all of the combinations of PC and diethyl carbonate (DEC) tested.[126] Many other studies report similar results with both layered oxide and polyanion positive electrodes.[127–130] The corrosion of aluminum, which starts at 3.3 to 3.5 V versus Na/Na^+, is a problem for NaOTf and NaTFSI salts (as for their Li counterparts). Sodium perchlorate or hexafluorophosphate allow an increase of the voltage window up to 5 V;[126,130,131] even small quantities of $NaPF_6$ efficiently passivate aluminum surfaces, thereby allowing the use of the TFSI anion.[126,131] For the same solvent and salt concentration, the ionic conductivity is slightly higher for $NaPF_6$-based electrolytes than NaTFSI electrolytes, with $NaClO_4$ being intermediate.[130,131] This is explained by the lower polarizing nature of the hexafluorophosphate anion.[132] Optimization of the solvent composition to lower viscosity results in conductivities of about 12 mS cm^{-1}, which is comparable with the best Li electrolytes.[131]

Hard carbon is the only anode material that has been systematically studied against different electrolytes, but the results are contradictory. Ponrouch et al. report very little influence of the salt ($NaClO_4$ or $NaPF_6$) on both the cycling performance of hard carbon electrodes and the nature of the SEI in PC, EC/PC, and EC/PC/DMC mixtures,[127] and a particularly high irreversible capacity was found in the case of 1M $NaClO_4$ in EC/DMC (50:50 wt%).[131] Another report shows good retention of capacity in EC/DMC (50:50 vol%) with both $NaPF_6$ and $NaClO_4$, and with a much superior behavior of the latter salt in PC solutions.[133]

The discrepancies show the high degree of sensitivity to the nature of the electrode and highlight the necessity of more work to fully characterize these systems.

A study on additives for $NaClO_4$ in PC has shown that vinylene carbonate (VC)—an important additive in Li electrolytes—does not efficiently passivate sodiated hard carbon electrodes.[129] The same study identified FEC as a very-efficient film-forming additive. Most interestingly, the same additive was successfully used with a variety of different anode materials, thus showing its good versatility.[134–136]

6.2. Ionic Liquids

To improve the safety of batteries, much effort has been devoted to reducing the volatility and flammability of organic liquid electrolytes. In this regard, ionic liquids (ILs) may help to address the safety problem as they are practically non-flammable (Figure 15).

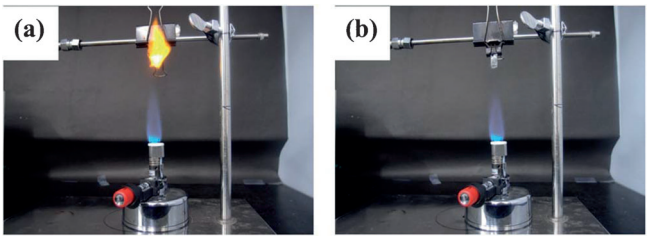

Figure 15. Flammability tests of a) conventional organic electrolyte and b) BMP-TFSI IL electrolyte with 1 M NaTFSI. Reproduced from Ref. [138] with permission, Copyright 2014, The Royal Society of Chemistry.

However, ILs usually require higher operating temperatures than liquid electrolytes because of their high viscosity, and melting points which are often just barely above room temperature. The only report of using an IL electrolyte with a practical anode material such as hard carbon shows good compatibility with a NaTFSI-doped *N*-methyl-*N*-propylpyrrolidinium bis(fluorosulfonyl)imide (NaFSI-C_1C_3pyrFSI) electrolyte at 90 °C.[137] Apart from this, most studies involve Na metal anodes. ILs such as 1-butyl(propyl)-1-methylpyrrolidinium bis(trifluoromethylsulfonyl)imide ([$C_4(C_3)$mpyr][TFSI]) doped with NaTFSI are able to reversibly strip and deposit sodium at room temperature.[138–140] A moderate overpotential of only 0.2 V for sodium electrodeposition was measured at room temperature; traces of water in the electrolyte were detrimental.[138,139] A voltage window of 5.2 V versus Na/Na^+ was reported together with good compatibility with the layered oxide cathode material $NaCrO_2$.[140]

Compatibility of the polyanion cathode material $NaFePO_4$ with the NaTFSI-doped [C_4mpyr][TFSI] electrolyte was also demonstrated in half cells.[141] Comparison with a similar cell operated in a 1M $NaClO_4$ in an EC/DEC electrolyte shows that although the non-aqueous electrolyte performs much better at room temperature, the IL electrolyte displays very similar capacity and rate capability at temperatures as low as 50 °C. In addition to the improved thermal stability of the IL electrolyte (> 400 °C), a much better cycle retention of 87 % after 100 cycles was reported, compared to only 62 % for the liquid electrolyte.

Substitution of the TFSI anion by the FSI (bis(fluorosulfonyl)imide) anion allows a further decrease of the temperature. Half-cells assembled with $Na_{0.45}Ni_{0.22}Co_{0.11}Mn_{0.66}O_2$ as the positive electrode and either a NaTSFI-doped [C_4mpyr][FSI] ionic liquid electrolyte or 0.5 M $NaPF_6$ in a PC-based non-aqueous electrolyte were compared. The reversible capacity at a rate of C/10 is slightly higher in the IL case,[142] with a good retention of 80 % of the capacity after 100 cycles, much higher than the non-aqueous cell.

Other promising ionic liquids have yet to be tested for battery applications.[143] The published results show that when safety is a more important parameter than rate capability, ionic liquid electrolytes are a superior choice to traditional non-aqueous electrolytes, even for room-temperature applications.

7. Summary and Outlook

As a consequence of concerns over the future cost of lithium and the sustainability of the resources, there is now a global trend to develop low-cost batteries with high energy densities that can meet a variety of emerging applications. Sodium ion batteries have re-emerged as promising candidates, especially for stationary energy storage. New directions have evolved beyond molten Na cells based on Na-S and Na-$NiCl_2$ that were developed in the last decade. They include aqueous Na ion cells, and the fast-developing field of non-aqueous batteries that could employ a plethora of newly discovered materials for the positive and negative electrodes as well as the electrolyte. These offer not only advantages of element sustainability, but present structural and electrochemical differences compared to their Li analogues that can be highly beneficial. This opens up a fascinating area of solid-state electrochemistry, which is ripe for exploration.

In terms of ambient-temperature cells that operate on the basis of intercalation chemistry, the last two years have witnessed several breakthroughs in the development of layered sodium transition-metal oxides as positive electrode materials, such as P2-$Na_{2/3}[Fe_{0.5}Mn_{0.5}]O_2$. These results suggest these sodium compounds can compete with their lithium analogues in terms of energy density. These exciting advances suggest the promise of large-scale cells even for vehicle electrification. Importantly, sodium and lithium compounds are not strictly or typically isostructural. Different electrochemical properties result and intriguing differences have emerged between the Li^+ and Na^+ layered metal oxides. These are the consequence of the larger Na^+ ion, which results in more highly ordered systems and less alkali-metal/transition-metal mixing on cycling, which is beneficial. A drawback is that many of the layered sodium metal oxides exhibit only moderate cycling stability at present, attributed to large volume changes on redox and a proclivity to P(n)–O(n) phase transitions induced by gliding of the transition-metal MO_2 layers. This results from the ability of Na^+ to adopt both octahedral and prismatic coordination, which is not the case for Li^+. Although these gliding transitions are not fully understood at present, they do represent a non-topotactic

process that could limit electrochemical reversibility. On the other hand, the tendency of Na^+ to not adopt tetrahedral coordination (unlike Li^+) means that transition to a spinel structure on partial desodiation from $NaMO_2$ is not favored as it is for some $LiMO_2$ compositions where it causes loss of capacity on cycling. Improved cycling stability can be attained by elemental substitution to suppress the phase transitions and reduce volume changes. These remain as hurdles to overcome for long-term cycle life. From a practical point of view, some sodium metal oxides exhibit a high sensitivity to moisture, although O3 phases have the advantage of full sodium content (meaning a nonsodiated anode can be used), and less air sensitivity. Another major advance is the very recent discovery of sodium-based "high-voltage" layered oxides, although it remains to be seen whether cycling stability will be achieved in this class of materials.

The larger size of Na^+ is also a factor for polyanion cathode materials, where the influence of the alkali metal size/charge ratio is significant in determining the thermodynamically most stable phase. These often have no lithium analogue. Advances have been realized with several novel, exciting polyanion materials: examples include $Na_{1.5}VPO_{4.8}F_{0.7}$ and, most recently, $Na_2Fe_2(SO_4)_3$. The latter exhibits a remarkably high Fe^{3+}/Fe^{2+} redox potential of 3.8 V versus Na, along with fast rate kinetics that are shared by the former. Although sulfate increases the redox potential, it also conveys moisture sensitivity: a disadvantage not shared by the relatively more stable phosphate-type materials. Intriguingly, for many polyanion materials, numerous modeling studies have revealed that the activation energy for Na^+ ion hopping is usually lower than for Li^+ (because of less polarization), with values being routinely as low as 0.3 eV. This provides distinct advantages for ion mobility, thus explaining the fast rate kinetics. The development of new unique sodium ion polyanion framework types will be pivotal for the advancement of the field of Na ion batteries. As the chemistry of Na intercalation is much less advanced than its lithium counterpart, much remains to be explored. This also means overcoming the disadvantage of the larger volume expansion/contraction afforded by the sodium cation with clever design of solid-state structures. We note that this challenge is common to both sodium metal polyanion and layered metal oxide systems, but less so for the more open Prussian blue framework solids, which present their own special opportunities.

New developments in negative electrode materials show that not only hard carbons, but graphitic materials can act as active Na ion intercalation compounds at low potential. Much scope lies in this area. Sodium metal dioxides based on titanium also show much promise. It is also worth noting that because Na does not alloy with aluminum (as does Li), this allows Al foil to be used as a current collector at the negative electrode rather than Cu. This is beneficial in terms of both cost and energy density. The generally lower voltage of Na compounds also provides considerable advantages for the development of the negative electrode. The potential of the sodium-containing positive electrode is similarly lowered, thus providing opportunities to explore materials where the lithium analogues have too high a potential to support many conventional electrolytes.

Overall, it is clear that Na ion batteries can compete with Li ion batteries in several important respects, but the sodium ion battery is still a very immature technology for energy storage applications compared to Li ion. Aside from the Na/S and ZEBRA high-temperature systems, no commercialized non-aqueous Na ion energy storage batteries exist at present. There is much opportunity for research and development. Many inroads have been made recently in developing new promising positive electrode materials. Finding good negative electrode materials remains a significant challenge. Nonetheless, compositions encompassing low-cost transition metals such as Fe, Mn, and Ti for either the positive or negative electrodes in Na ion rechargeable battery systems, without sacrificing high energy density and high power, are now within scope. This paves way for the discovery of new sustainable cathodes made with earth-abundant elements for large-scale batteries.

Acknowledgements

This research was supported by the Natural Sciences and Engineering Council of Canada through their Discovery and Canada Research Chair programs. L.F.N. gratefully acknowledges their ongoing support for new electrochemical technologies.

Received: October 23, 2014
Published online: February 4, 2015

[1] J. M. Tarascon, M. Armand, *Nature* **2001**, *414*, 359 – 367.
[2] F. Risacher, B. Fritz, *Aquat. Geochem.* **2009**, *15*, 123 – 157.
[3] A. Yaksic, J. E. Tilton, *Resour. Policy* **2009**, *34*, 185 – 194.
[4] S. Fletcher, *Bottled Lightning: Superbatteries, Electric Cars, and the New Lithium Economy*, Hill and Wang, New York, **2012**.
[5] Y.-F. Y. Yao, J. T. Kummer, *J. Inorg. Nucl. Chem.* **1967**, *29*, 2453 – 2459.
[6] J. B. Goodenough, H. Y.-P. Hong, J. A. Kafalas, *Mater. Res. Bull.* **1976**, *11*, 203 – 220.
[7] Ceramatec, Inc. WO2012061823A2, patent application, **2012**.
[8] A. Hayashi, K. Noi, A. Sakuda, M. Tatsumisago, *Nat. Commun.* **2012**, *3*, 856.
[9] V. Palomares, P. Serras, I. Villaluenga, K. B. Hueso, J. Carretero-Gonzalez, T. Rojo, *Energy Environ. Sci.* **2012**, *5*, 5884 – 5901; V. Palomares, M. Casas-Cabanas, E. Castillo-Martinez, M. H. Han, T. Rojo, *Energy Environ. Sci.* **2013**, *6*, 2312 – 2337.
[10] S. W. Ki, D.-H. Seo, X. Ma, G. Ceder, K. Kang, *Adv. Energy Mater.* **2012**, *2*, 710 – 721.
[11] H. Pan, Y. S. Hu, L. Chen, *Energy Environ. Sci.* **2013**, *6*, 2338 – 2360.
[12] M. D. Slater, D. Kim, E. Lee, C. S. Johnson, *Adv. Funct. Mater.* **2013**, *23*, 947 – 958.
[13] H. Kim, J. Hong, K.-Y. Park, H. Kim, S.-W. Kim, K. Kang, *Chem. Rev.* **2014**, *114*, 11788 – 11827.
[14] H. Böhm, G. Beyermann, *J. Power Sources* **1999**, *84*, 270 – 274.
[15] R. C. Galloway, S. Haslam, *J. Power Sources* **1999**, *80*, 164 – 170.
[16] T. Javadi, A. Petric, *J. Electrochem. Soc.* **2011**, *158*, A700 – A704.
[17] T. M. O. Sullivan, C. M. Bingham, R. E. Clark, *International Symposium on Power Electronics, Electric Drives, Automation and Motion*, **2006**, pp. 34 – 36.
[18] A. van Zyl, *Solid State Ionics* **1996**, *86*, 883 – 889.

[19] D. J. L. Brett, P. Aguiar, N. P. Brandon, *J. Power Sources* **2006**, *163*, 514 – 522.
[20] M. S. Whittingham, *Prog. Solid State Chem.* **1978**, *12*, 41 – 99.
[21] A. S. Nagelberg, W. L. Worrell, *J. Solid State Chem.* **1979**, *29*, 345 – 354.
[22] T. Ohzuku, A. Ueda, M. Nagayama, Y. Iwakoshi, H. Komori, *Electrochim. Acta* **1993**, *38*, 1159 – 1167.
[23] K. Ozawa, *Solid State Ionics* **1994**, *69*, 212 – 216.
[24] R. Yazami, N. Lebrun, M. Bonneau, M. Molteni, *J. Power Sources* **1995**, *54*, 389 – 392.
[25] T. Ohzuku, Y. Makimura, *Chem. Lett.* **2001**, *8*, 744 – 745.
[26] R. Berthelot, D. Carlier, C. Delmas, *Nat. Mater.* **2011**, *10*, 74 – 80.
[27] D. Carlier, J. H. Cheng, R. Berthelot, M. Guignard, M. Yoncheva, R. Stoyanova, et al., *Dalton Trans.* **2011**, *40*, 9306 – 9312.
[28] J.-P. Parant, R. Olazcuaga, M. Devalette, C. Fouassier, *J. Solid State Chem.* **1971**, *3*, 1 – 11.
[29] A. Mendiboure, C. Delmas, P. Hagenmuller, *J. Solid State Chem.* **1985**, *57*, 323 – 331.
[30] O. I. Velikokhatnyi, C.-C. Chang, P. N. Kumta, *J. Electrochem. Soc.* **2003**, *150*, A1262 – 1266.
[31] X. Ma, H. Chen, G. Ceder, *J. Electrochem. Soc.* **2011**, *158*, A1307 – 1311.
[32] N. Yabuuchi, M. Kajiyama, J. Iwatate, H. Nishikawa, S. Hitomi, R. Okuyama, R. Usui, Y. Yamada, S. Komaba, *Nat. Mater.* **2012**, *11*, 512 – 517.
[33] Ref. [26].
[34] H. Tomita, K. Kubota, R. Kanno, *J. Power Sources* **2011**, *196*, 6809 – 6814.
[35] J. Xu, D. H. Lee, R. J. Clément, X. Yu, M. Leskes, A. J. Pell, G. Pintacuda, X.-Q. Yang, C. P. Grey, Y. S. Meng, *Chem. Mater.* **2014**, *26*, 1260 – 1269.
[36] N. Yabuuchi, R. Hara, M. Kajiyama, K. Kubota, T. Ishigaki, A. Hoshikawa, S. Komaba, *Adv. Energy Mater.* **2014**, *4*, 1301453.
[37] a) Y.-K. Sun, Z. Chen, H.-J. Noh, D.-J. Lee, H.-G. Jung, Y. Ren, S. Wang, C. Seung Yoon, S.-T. Myung, K. Amine, *Nat. Mater.* **2012**, *11*, 942 – 947; b) D. Wang, I. Belharouak, G. Zhou, K. Amine, *Adv. Funct. Mater.* **2013**, *23*, 1070 – 1075.
[38] D. Mohanty, A. Huq, E. A. Payzant, A. S. Sefat, J. Li, D. P. Abraham, D. L. Wood, C. Daniel, *Chem. Mater.* **2013**, *25*, 4064 – 4070.
[39] J. Billaud, G. Singh, A. R. Armstrong, E. Gonzalo, V. Roddatis, M. Armand, T. Rojo, P. G. Bruce, *Energy Environ. Sci.* **2014**, *7*, 1387 – 1391.
[40] N. Yabuuchi, R. Hara, K. Kubota, J. Paulsen, S. Kumakura, S. Komaba, *J. Mater. Chem. A* **2014**, *2*, 16851 – 16855.
[41] S. LeVine, *The Powerhouse: Inside the Invention of a Battery to Save the World*, Viking Adult, Penguin Random House, Canada, **2015**.
[42] D. Kim, E. Lee, M. Slater, W. Lu, S. Rood, C. S. Johnson, *Electrochem. Commun.* **2012**, *18*, 66 – 69.
[43] X. Wang, G. Liu, T. Iwao, M. Okubo, A. Yamada, *J. Phys. Chem. C* **2014**, *118*, 2970 – 2976.
[44] Z. Lu, J. R. Dahn, *Chem. Mater.* **2001**, *13*, 1252 – 1257.
[45] D. Buchholz, L. G. Chagas, C. Vaalma, L. Wu, S. Passerini, *J. Mater. Chem. A* **2014**, *2*, 13415 – 13421.
[46] M. Sathiya, K. Hemalatha, K. Ramesha, J. M. Tarascon, A. S. Prakash, *Chem. Mater.* **2012**, *24*, 1846 – 1853.
[47] E. Talaie, V. Duffort, L. F. Nazar, submitted.
[48] P. Moreau, D. Guyomard, J. Gaubicher, F. Boucher, *Chem. Mater.* **2010**, *22*, 4126 – 4128.
[49] P. P. Prosini, C. Centoa, A. Masci, M. Carewska, *Solid State Ionics* **2014**, *263*, 1 – 8.
[50] K. T. Lee, T. N. Ramesh, F. Nan, G. Botton, L. F. Nazar, *Chem. Mater.* **2011**, *23*, 3593 – 3600.
[51] S. M. Oh, S. T. Myung, J. Hassoun, B. Scrosati, Y. K. Sun, *Electrochem. Commun.* **2012**, *22*, 149 – 152.
[52] J. Lu, S. C. Chung, S. Nishimura, A. Yamada, *Chem. Mater.* **2013**, *25*, 4557 – 4565.
[53] R. Tripathi, S. M. Wood, M. S. Islam, L. F. Nazar, *Energy Environ. Sci.* **2013**, *6*, 2257 – 2265.
[54] H. Liu, F. C. Strobridge, O. J. Borkiewicz, K. M. Wiaderek, K. W. Chapman, P. J. Chupas, C. P. Grey, *Science* **2014**, *334*, 1252817-1 – 1252817-7.
[55] X. Zhang, M. van Hulzen, D. P. Singh, A. Brownrigg, J. P. Wright, N. H. van Dijk, M. Wagemaker, *Nano Lett.* **2014**, *14*, 2279 – 2285.
[56] K. Saravanan, C. W. Mason, A. Rudola, K. H. Wong, P. Balaya, *Adv. Energy Mater.* **2013**, *3*, 444 – 450.
[57] C. Zhu, K. Song, P. A. van Aken, J. Maier, Y. Yu, *Nano Lett.* **2014**, *14*, 2175 – 2180.
[58] J. Liu, K. Tang, K. Song, P. A. van Aken, Y. Yu, J. Maier, *Nanoscale* **2014**, *6*, 5081 – 5086.
[59] R. A. Shakoor, D. H. Seo, H. Kim, Y. U. Park, J. Kim, S. W. Kim, H. Gwon, S. Leec, K. Kang, *J. Mater. Chem.* **2012**, *22*, 20535 – 20541.
[60] W. Song, X. Ji, Z. Wu, Y. Zhu, F. Li, Y. Yao, C. E. Banks, *RSC Adv.* **2014**, *4*, 11375 – 11383.
[61] B. L. Ellis, W. R. M. Makhanouk, Y. Makimura, K. Toughilland, L. F. Nazar, *Nat. Mater.* **2007**, *6*, 749 – 753.
[62] Y. U. Park, D. H. Seo, H. S. Kwon, B. Kim, J. Kim, H. Kim, I. Kim, H. I. Yoo, K. Kang, *J. Am. Chem. Soc.* **2013**, *135*, 13870 – 13878.
[63] N. Recham, J.-N. Chotard, L. Dupont, K. Djellab, M. Armand, J-M. Tarascon, *J. Electrochem. Soc.* **2009**, *156*, A993 – A999.
[64] Y. Kawabe, N. Yabuuchi, M. Kajiyama, N. Fukuhara, T. Inamasu, R. Okuyama, I. Nakai, S. Komaba, *Electrochem. Commun.* **2011**, *13*, 1225 – 1228.
[65] B. Ellis, D. H. Ryan, L. F. Nazar, *Chem. Mater.* **2010**, *22*, 1059 – 1070.
[66] P. Barpanda, G. Liu, C. D. Ling, M. Tamaru, M. Avdeev, S. C. Chung, Y. Yamada, A. Yamada, *Chem. Mater.* **2013**, *25*, 3480 – 3487.
[67] P. Barpanda, T. Ye, M. Avdeev, S. C. Chunga, A. Yamada, *J. Mater. Chem. A* **2013**, *1*, 4194 – 4197.
[68] P. Barpanda, J. Lu, T. Ye, M. Kajiyama, S. C. Chung, N. Yabuuchi, S. Komaba, A. Yamada, *RSC Adv.* **2013**, *3*, 3857 – 3860.
[69] J. Pizarro-Sanz, J. Dance, G. Villeneuve, M. Arriortua-Marcaida, *Mater. Lett.* **1994**, *18*, 327 – 332.
[70] R. Tripathi, T. N. Ramesh, B. L. Ellis, L. F. Nazar, *Angew. Chem. Int. Ed.* **2010**, *49*, 8738 – 8742; *Angew. Chem.* **2010**, *122*, 8920 – 8924.
[71] P. Barpanda, J.-N. Chotard, N. Recham, C. Delacourt, M. Ati, L. Dupont, M. Armand, J.-M. Tarascon, *Inorg. Chem.* **2010**, *49*, 7401 – 7408.
[72] R. Tripathi, G. R. Gardiner, M. S. Islam, L. F. Nazar, *Chem. Mater.* **2011**, *23*, 2278 – 2288.
[73] M. Reynaud, G. Rousse, A. M. Abakumov, M. T. Sougrati, G. V. Tendeloo, J. N. Chotarda, J. M. Tarascon, *J. Mater. Chem. A* **2014**, *2*, 2671 – 2680.
[74] P. Barpanda, G. Oyama, C. D. Ling, A. Yamada, *Chem. Mater.* **2014**, *26*, 1297 – 1299.
[75] P. Barpanda, G. Oyama, S. Nishimura, S. C. Chung, A. Yamada, *Nat. Commun.* **2014**, *5*, 4358.
[76] J. Liu, D. Chang, P. Whitfield, Y. Janssen, X. Yu, Y. Zhou, J. Bai, J. Ko, K. W. Nam, L. Wu, Y. Zhu, M. Feygenson, G. Amatucci, A. V. Ven, X. Q. Yang, P. Khalifah, *Chem. Mater.* **2014**, *26*, 3295 – 3305.
[77] H. Chen, Q. Hao, O. Zivkovic, G. Hautier, L. S. Du, Y. Tang, Y. Y. Hu, X. Ma, C. P. Grey, G. Ceder, *Chem. Mater.* **2013**, *25*, 2777 – 2786.

[78] W. Huang, J. Zhou, B. Li, J. Ma, S. Tao, D. Xia, W. Chu, Z. Wu, *Sci. Rep.* **2014**, *4*, 1 – 8.
[79] H. J. Buser, D. Schwarzenbach, W. Petter, A. Ludi, *Inorg. Chem.* **1977**, *16*, 2704 – 2709.
[80] Y. Lu, L. Wang, J. Cheng, J. B. Goodenough, *Chem. Commun.* **2012**, *48*, 6544 – 6546.
[81] H. Lee, Y.-I. Kim, J.-K. Park, J. W. Choi, *Chem. Commun.* **2012**, *48*, 8416 – 8418.
[82] a) T. Matsuda, M. Takachi, Y. Moritomo, *Chem. Commun.* **2013**, *49*, 2750 – 2752; b) M. Takachi, T. Matsuda, Y. Moritomo, *Jpn. J. Appl. Phys.* **2013**, *52*, 090202.
[83] Y. Yue, A. J. Binder, G. Guo, A. Zhang, Z.-A. Qiao, C. Tian, S. Dai, *Angew. Chem. Int. Ed.* **2014**, *53*, 3134 – 3137; *Angew. Chem.* **2014**, *126*, 3198 – 3201.
[84] L. Wang, Y. Lu, J. Liu, M. Xu, J. Cheng, D. Zhang, J. B. Goodenough, *Angew. Chem. Int. Ed.* **2013**, *52*, 1964 – 1969; *Angew. Chem.* **2013**, *125*, 2018 – 2021.
[85] X. Wu, W. Deng, J. Qian, Y. Cao, X. Ai, H. Yang, *J. Mater. Chem. A* **2013**, *1*, 10130.
[86] Y. You, X.-L. Wu, Y.-X. Yin, Y.-G. Guo, *Energy Environ. Sci.* **2014**, *7*, 1643 – 1647.
[87] H.-W. Lee, R. Y. Wang, M. Pasta, S. W. Lee, N. Liu, Y. Cui, *Nat. Commun.* **2014**, *5*, 5280.
[88] M. S. Islam, C. A. J. Fisher, *Chem. Soc. Rev.* **2014**, *43*, 185 – 204.
[89] S. P. Ong, V. L. Chevrier, G. Hautier, A. Jain, C. Moore, S. Kim, X. Ma, G. Ceder, *Energy Environ. Sci.* **2011**, *4*, 3680.
[90] H. Kim, D. J. Kim, D.-H. Seo, M. S. Yeom, K. Kang, D. K. Kim, Y. Jung, *Chem. Mater.* **2012**, *24*, 1205 – 1211.
[91] D. H. Lee, J. Xu, Y. S. Meng, *Phys. Chem. Chem. Phys.* **2013**, *15*, 3304 – 3312.
[92] Y. Hinuma, Y. S. Meng, G. Ceder, *Phys. Rev. B* **2008**, *77*, 224111.
[93] Y. Mo, S. P. Ong, G. Ceder, *Chem. Mater.* **2014**, *26*, 5208 – 5214.
[94] Ref. [53].
[95] J. M. Clark, P. Barpanda, A. Yamada, M. Saiful Islam, *J. Mater. Chem. A* **2014**, *2*, 11807 – 11812.
[96] I. A. Udod, H. B. Orman, V. K. Genchel, *Carbon* **1994**, *32*, 101 – 106.
[97] M. M. Doeff, Y. Ma, S. J. Visco, L. C. De Jonghe, *J. Electrochem. Soc.* **1993**, *140*, L169 – L170.
[98] a) D. A. Stevens, J. R. Dahn, *J. Electrochem. Soc.* **2000**, *147*, 1271 – 1273; b) D. A. Stevens, J. R. Dahn, *J. Electrochem. Soc.* **2001**, *148*, A803.
[99] S. Komaba, W. Murata, T. Ishikawa, N. Yabuuchi, T. Ozeki, T. Nakayama, A. Ogata, K. Gotoh, K. Fujiwara, *Adv. Funct. Mater.* **2011**, *21*, 3859 – 3867.
[100] R. C. Asher, *J. Inorg. Nucl. Chem.* **1959**, *10*, 238 – 249.
[101] P. Ge, M. Fouletier, *Solid State Ionics* **1988**, *28 – 30*, 1172 – 1175.
[102] S. Komaba, T. Ishikawa, N. Yabuuchi, W. Murata, A. Ito, Y. Ohsawa, *ACS Appl. Mater. Interfaces* **2011**, *3*, 4165 – 4168.
[103] S. Wenzel, T. Hara, J. Janek, P. Adelhelm, *Energy Environ. Sci.* **2011**, *4*, 3342 – 3348.
[104] Y. Wen, K. He, Y. Zhu, F. Han, Y. Xu, I. Matsuda, Y. Ishii, J. Cumings, C. Wang, *Nat. Commun.* **2014**, *5*, 4033.
[105] Y.-X. Wang, S.-L. Chou, H.-K. Liu, S.-X. Dou, *Carbon* **2013**, *57*, 202 – 208.
[106] S. I. Park, I. Gocheva, S. Okada, J. Yamaki, *J. Electrochem. Soc.* **2011**, *158*, A1067.
[107] C. Didier, M. Guignard, C. Denage, O. Szajwaj, S. Ito, I. Saadoune, J. Darriet, C. Delmas, *Electrochem. Solid-State Lett.* **2011**, *14*, A75 – A78.
[108] M. Guignard, C. Didier, J. Darriet, P. Bordet, E. Elkaïm, C. Delmas, *Nat. Mater.* **2013**, *12*, 74 – 80.
[109] H. Xiong, M. D. Slater, M. Balasubramanian, C. S. Johnson, T. Rajh, *J. Phys. Chem. Lett.* **2011**, *2*, 2560 – 2565.
[110] P. Senguttuvan, G. Rousse, V. Seznec, J.-M. Tarascon, M. R. Palacín, *Chem. Mater.* **2011**, *23*, 4109 – 4111.
[111] W. Wang, C. Yu, Z. Lin, J. Hou, H. Zhu, S. Jiao, *Nanoscale* **2013**, *5*, 594 – 599.
[112] A. Rudola, K. Saravanan, C. W. Mason, P. Balaya, *J. Mater. Chem. A* **2013**, *1*, 2653 – 2662.
[113] B. Guo, X. Yu, X.-G. Sun, M. Chi, Z.-A. Qiao, J. Liu, Y.-S. Hu, X.-Q. Yang, J. B. Goodenough, S. Dai, *Energy Environ. Sci.* **2014**, *7*, 2220 – 2226.
[114] Y. Wang, X. Yu, S. Xu, J. Bai, R. Xiao, Y.-S. Hu, H. Li, X.-Q. Yang, L. Chen, X. Huang, *Nat. Commun.* **2013**, *4*, 2365.
[115] R. Fielden, M. N. Obrovac, *J. Electrochem. Soc.* **2014**, *161*, A1158 – A1163.
[116] V. L. Chevrier, G. Ceder, *J. Electrochem. Soc.* **2011**, *158*, A1011 – A1014.
[117] S. Komaba, Y. Matsuura, T. Ishikawa, N. Yabuuchi, W. Murata, S. Kuze, *Electrochem. Commun.* **2012**, *21*, 65 – 68.
[118] L. D. Ellis, B. N. Wilkes, T. D. Hatchard, M. N. Obrovac, *J. Electrochem. Soc.* **2014**, *161*, A416 – A421.
[119] T. T. Tran, M. N. Obrovac, *J. Electrochem. Soc.* **2011**, *158*, A1411 – A1416.
[120] J. W. Wang, X. H. Liu, S. X. Mao, J. Y. Huang, *Nano Lett.* **2012**, *12*, 5897 – 5902.
[121] L. D. Ellis, T. D. Hatchard, *M. N. Obrovac, J. Electrochem. Soc.* **2012**, *159*, A1801 – A1805.
[122] Z. Du, R. A. Dunlap, M. N. Obrovac, *J. Alloys Compd.* **2014**, *617*, 271 – 276.
[123] A. Darwiche, C. Marino, M. T. Sougrati, B. Fraisse, L. Stievano, L. Monconduit, *J. Am. Chem. Soc.* **2012**, *134*, 20805 – 20811.
[124] J. Qian, X. Wu, Y. Cao, X. Ai, H. Yang, *Angew. Chem. Int. Ed.* **2013**, *52*, 4633 – 4636; *Angew. Chem.* **2013**, *125*, 4731 – 4734.
[125] Ref. [8].
[126] T. D. Hatchard, M. N. Obrovac, *J. Electrochem. Soc.* **2014**, *161*, A1748 – A1752.
[127] A. Ponrouch, R. Dedryvere, D. Monti, A. E. Demet, J. M. Ateba Mba, L. Croguennec, C. Masquelier, P. Johansson, M. R. Palacin, *Energy Environ. Sci.* **2013**, *6*, 2361 – 2369.
[128] Ref. [99].
[129] Ref. [102].
[130] A. Bhide, J. Hofmann, A. K. Durr, J. Janek, P. Adelhelm, *Phys. Chem. Chem. Phys.* **2014**, *16*, 1987 – 1998.
[131] A. Ponrouch, E. Marchante, M. Courty, J.-M. Tarascon, M. R. Palacin, *Energy Environ. Sci.* **2012**, *5*, 8572 – 8583.
[132] J. M. Tarascon, D. Guyomard, *Solid State Ionics* **1994**, *69*, 293 – 305.
[133] J. Zhao, L. Zhao, K. Chihara, S. Okada, J.-i. Yamaki, S. Matsumoto, S. Kuze, K. Nakane, *J. Power Sources* **2013**, *244*, 752 – 757.
[134] Ref. [117].
[135] Ref. [123].
[136] Ref. [124].
[137] A. Fukunaga, T. Nohira, R. Hagiwara, K. Numata, E. Itani, S. Sakai, K. Nitta, S. Inazawa, *J. Power Sources* **2014**, *246*, 387 – 391.
[138] S. A. Mohd Noor, P. C. Howlett, D. R. MacFarlane, M. Forsyth, *Electrochim. Acta* **2013**, *114*, 766 – 771.
[139] H. Yoon, H. Zhu, A. Hervault, M. Armand, D. R. MacFarlane, M. Forsyth, *Phys. Chem. Chem. Phys.* **2014**, *16*, 12350 – 12355.
[140] C. Ding, T. Nohira, K. Kuroda, R. Hagiwara, A. Fukunaga, S. Sakai, K. Nitta, S. Inazawa, *J. Power Sources* **2013**, *238*, 296 – 300.
[141] N. Wongittharom, T.-C. Lee, C.-H. Wang, Y.-C. Wang, J.-K. Chang, *J. Mater. Chem. A* **2014**, *2*, 5655 – 5661.
[142] L. G. Chagas, D. Buchholz, L. Wu, B. Vortmann, S. Passerini, *J. Power Sources* **2014**, *247*, 377 – 383.
[143] D. Monti, E. Jónsson, M. R. Palacín, P. Johansson, *J. Power Sources* **2014**, *245*, 630 – 636.

